Spatial-temporal distribution, photoreactivity and environmental control of dissolved organic matter in the sea-surface microlayer of the eastern marginal seas of China

Lin Yang [a], Jing Zhang [a, c, *], Anja Engel[d], Gui-Peng Yang [a, b, c, *]

[a] Frontiers Science Center for Deep Ocean Multispheres and Earth System, and Key Laboratory of Marine Chemistry Theory and Technology, Ministry of Education, Ocean University of China, Qingdao 266100, China

[b] Laboratory for Marine Ecology and Environmental Science, Qingdao National Laboratory for Marine Science and Technology, Qingdao 266237, China

[c] Institute of Marine Chemistry, Ocean University of China, Qingdao 266100, China

[d] GEOMAR Helmholtz Centre for Ocean Research, 24105 Kiel, Germany

[*] Corresponding authors. Key Laboratory of Marine Chemistry Theory and Technology, Ministry of Education, Ocean University of China, Qingdao 266100, China
E-mail addresses: zhangjouc@ouc.edu.cn (J. Zhang), gpyang@ouc.edu.cn (G.-P. Yang)

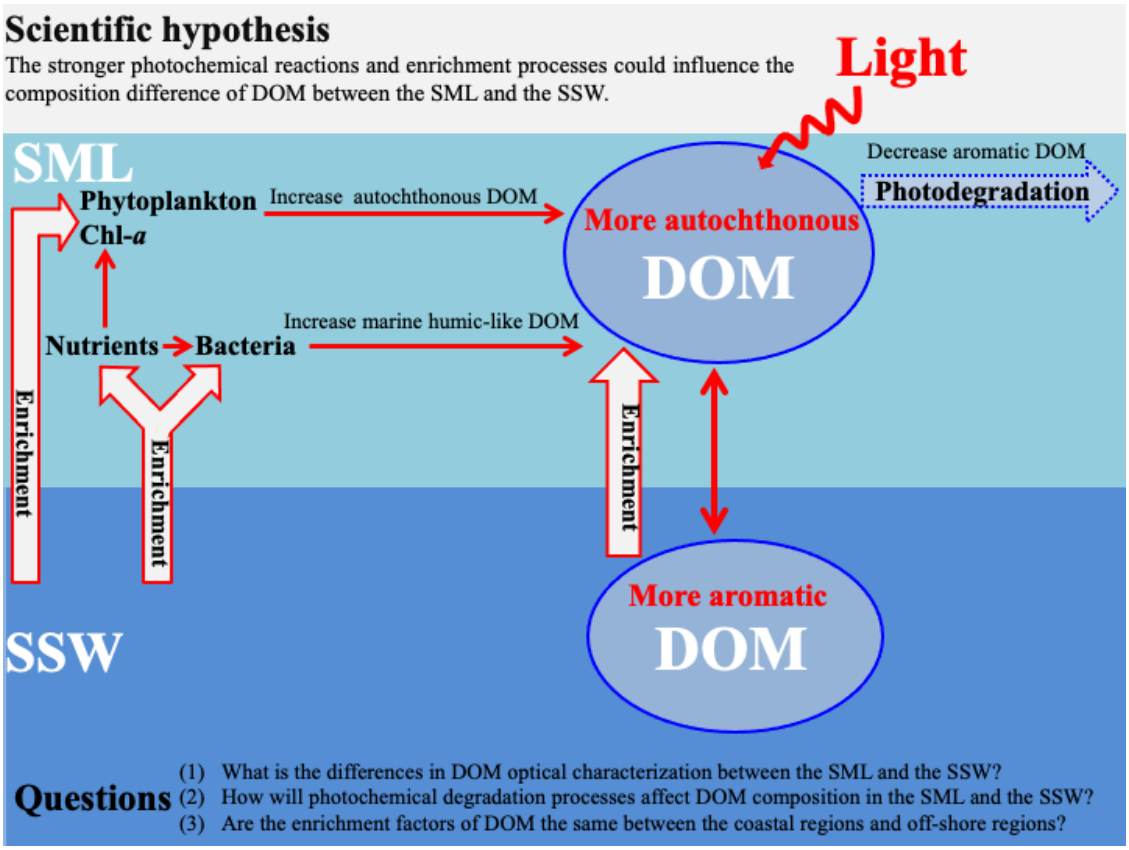

Graphical Abstract

Abstract

As the boundary interface between the atmosphere and ocean, the sea-surface microlayer (SML) plays a significant role in the biogeochemical cycles of dissolved organic matter (DOM) and macronutrients in marine environments. In our study, the optical properties of DOM were compared between the SSW and the SML during spring, summer and winter in the East China Sea (ECS) and the Yellow Sea (YS). In addition, photoexposure experiments were designed to compare photochemical degradation processes of DOM between the SML and the SSW. Chromophoric DOM (CDOM), fluorescent DOM, dissolved organic carbon, chlorophyll *a*, picoplankton, nutrients, and bacteria were frequently enriched in the SML. The enrichment factors (EFs) of tryptophan-like component 4 was significantly higher than other fluorescence components; the longer wavelength absorption values of CDOM showed higher EFs in the SML, and the more significant relationship between CDOM and Chl-a in the SML, indicating that autochthonous DOM was more strongly enriched in the SML than the terrestrial DOM. Higher EFs were generally observed in the SML in the off-shore regions than in the coastal regions, and CDOM in the SML was photobleached more after relatively strong irradiation, as also indicated by the lower percentages of humic-like DOM and lower specific UV absorbance values ($SUVA_{254}$) in the SML than the subsurface water (SSW). Compared to the SSW, the elevated nutrients may stimulate phytoplankton growth, biological activity and then production of abundant fresh autochthonous DOM in the SML. Our results revealed a new enrichment model for exploring the air-sea interface environment, which can explain the more autochthonous properties of DOM in the SML than the SSW.

Keywords: Sea-surface microlayer; Dissolved organic matter; Photochemical degradation;

Enrichment processes; Eastern marginal seas of China

1 Introduction

The sea-surface microlayer (SML) is the boundary interface between the atmosphere and the ocean, which covers about 70% of the Earth's surface. SML is physicochemically distinct from subsurface water (SSW, depth 3 ~ 5 m) and is characteristically enriched with phytoneuston, chlorophyll, particulate carbon, dissolved organic matter (Hardy 1982; Hardy and Apts, 1989), and biogenic organic compounds, such as lipids, proteins, and polysaccharides ((Liss and Duce, 1997; Liss and Duce, 2005). With a total thickness ranging between 1 μm and 1000 μm, the SML remains present in wind speeds of up to 13 m s^{-1} (Sabbaghzadeh et al., 2017). A variety of processes contribute to the formation of the SML in aquatic systems, these include but are not limited to, scavenging by rising bubbles, atmospheric deposition, dissolved organic matter (DOM) photochemical degradation and transformation, secretion, and biodegradation by organisms living within the microlayer (Neuston), and migration of motile organisms into the SML (Aller et al., 2005; Wotton and Preston, 2005). The SML is a very dynamic interface (Cunliffe et al., 2013), moreover, the impact of changes in UV radiation on air-sea fluxes in the SML of important trace gases need to be assessed. In addition, another uncertainty is whether photochemical reactions on the SML affect the flux of volatile species at the air-sea interface (Blough, 1997). Therefore, the role of the microlayer in oceanic emissions is not well understood and fundamental advance in understanding its properties are needed.

The processes leading to the enrichment of DOM in the SML are not solely controlled by changes in the DOM concentration at the sea surface microlayer, but are more complex (Mustaffa et al., 2018). Because of its unique position at the air-sea interface, the biological and photochemical reactions of DOM in the SML could strongly impact the biogeochemical cycling of biologically important

58 elements, for example, via the conversion of DOM into volatile species such as carbonyl sulfide
59 (OCS), which influence the atmospheric chemistry and climate (Mopper et al., 2002). Air-sea gas
60 exchanges of trace gases (e.g., CO, OCS, dimethylsulfide (DMS), and alkyl nitrates gases) can also be
61 greatly influenced by biological and photochemical reactions at the sea surface (Blough, 1997).

62 Optical measurements of absorbance and fluorescence have been applied to track DOM
63 variability in aquatic ecosystems (McKnight et al., 2001; Zepp et al., 2004; Coble, 2007). The fraction
64 of DOM that absorbs light in the ultraviolet and visible ranges of the electromagnetic spectrum and the
65 fraction that exhibits a blue fluorescence are known as chromophoric DOM (CDOM) and fluorescence
66 DOM (FDOM), respectively, and their relative compositions can provide information differentiating
67 between autochthonous and allochthonous sources (Coble, 1996; McKnight et al., 2001; Stedmon et
68 al., 2007). Photolysis of DOM promotes the formation of low-molecular-weight compounds,
69 increasing the bioavailability of biologically refractory materials and facilitating carbon uptake by
70 microbes (Kieber et al., 1989). Indices based on optical measurements of absorbance and fluorescence
71 are commonly used to track DOM composition and infer DOM processing due to their low analytical
72 cost and high throughput relative to molecular level analyses (Coble, 2007; Fellman et al., 2010;
73 Gabor et al., 2014). Recent studies have mainly focused on using the characteristics of CDOM as
74 indicators of the sources and degradation states of DOM (Massicotte et al., 2017) in the SSW, and its
75 vertical distribution in estuaries and open oceans (Yamashita et al., 2017; Margolin et al., 2018). In
76 addition, Mustaffa et al. (2018 and 2017) observed that FDOM enrichment in the SML in the coastal
77 regions and open Atlantic Ocean, and FDOM is frequently enriched during upwelling events in the
78 Baltic Sea.

79 Even though there are many studies that have documented the enrichment in DOM (e.g. amino

acids; carbohydrates) and inorganic nutrients in the SML relative to the SSW (Orellana et al., 2011; Chen et al., 2016), the differences in organic matter composition between the SML and SSW, the different enrichment factors of DOM in the SML between the coastal regions and the off-shore regions, and how do photochemical degradation activities regulate DOM concentration in the SML need more thorough discussion. Here, we investigated the concentration and composition of DOM in the SML relative to the SSW and the responses of DOM to photoexposure. We hypothesized that the photochemical reactions and enrichment processes could influence the composition difference of DOM between the SML and the SSW, and greater solar exposure in the SML than in the SSW would enhance the mineralization of DOM. To test these hypotheses, our study was designed to answer the questions: (1) What is the differences in optical characterization of DOM between the SML and the SSW? (2) Are the enrichment factors (EFs) of DOM the same between the coastal regions and off-shore regions? (3) How will photochemical degradation processes affect DOM composition in the SML and the SSW? We, therefore, compared the optical properties of DOM between the SSW and the SML, and EFs of CDOM, FDOM components, dissolved organic carbon (DOC), chlorophyll-*a* (Chl-*a*), nutrients, and bacterial abundance from the coastal waters to open ocean in the eastern marginal seas of China (including the East China Sea (ECS) and the Yellow Sea (YS)) during spring of 2017 and 2019, summer of 2018, and winter of 2019; discuss how the composition of accumulated DOM was affected by environmental conditions (wind speed and salinity) within the SML; and conducted photoexposure experiments to compare photochemical degradation processes of DOM between the SML and the SSW.

2 Materials and methods

2.1 Study Area

Four cruises were conducted during the four seasons, specifically, from: 27 March to 15 April 2017 (R/V "*Dong Fang Hong 2*"), 26 June to 19 July 2018 (R/V "*Dong Fang Hong 2*"), March 2019 (R/V "*Zheyu No. 2*"), and 28 December 2019 to 16 January 2020 (R/V "*Dong Fang Hong 3*"). The station locations are shown in Fig. 1. In spring, summer, and winter, SML samples were collected in the YS and the ECS, which are shallow seas located almost entirely on the continental shelf in the western Pacific Ocean where there is strong interaction between land and sea.

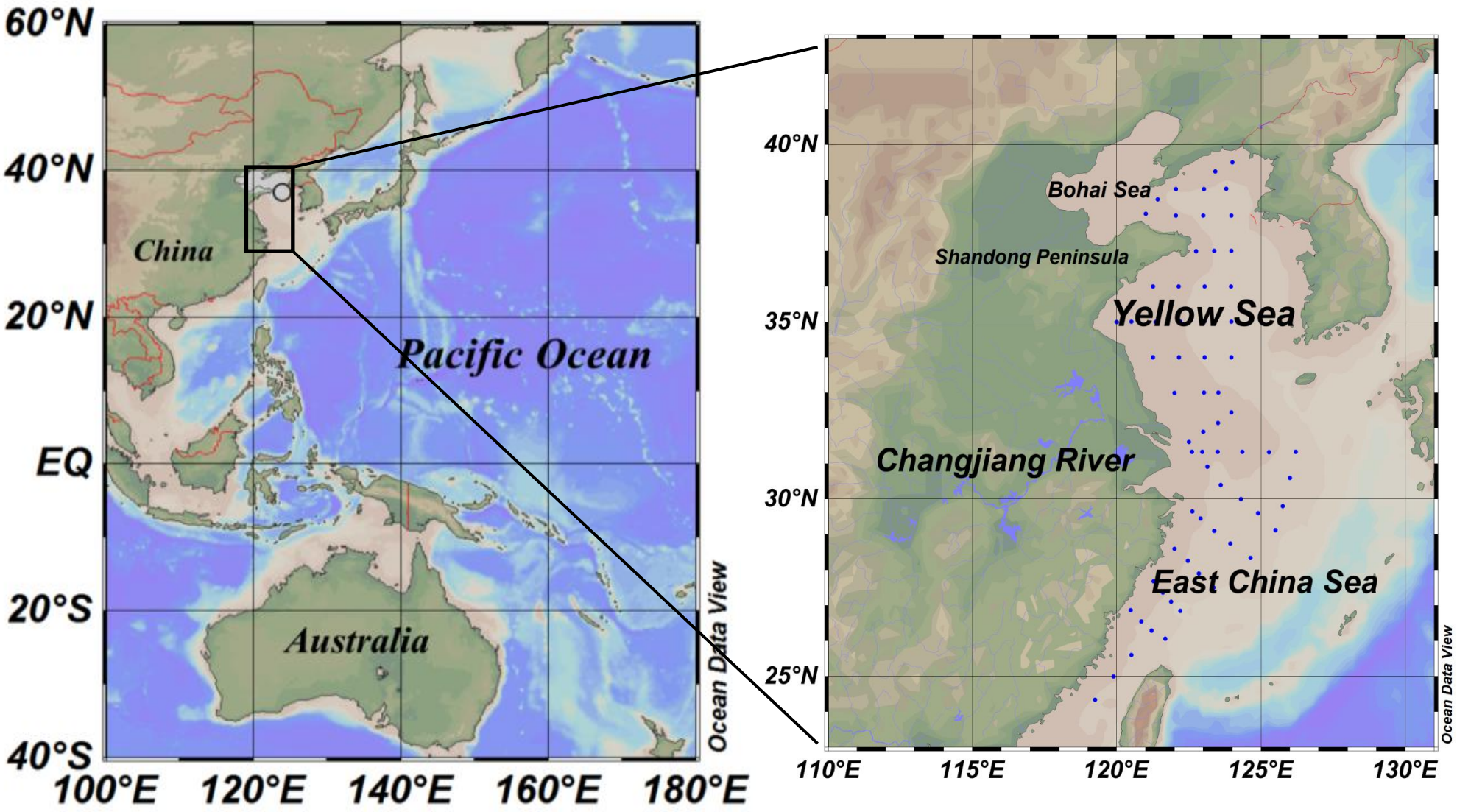
60°N
40°N
20°N
EQ
20°S
40°S
100°E
120°E
140°E
160°E
180°E
China
Pacific Ocean
Australia
Ocean Data View
40°N
35°N
30°N
25°N
110°E
115°E
120°E
125°E
130°E
Bohai Sea
Shandong Peninsula
Yellow Sea
Changjiang River
East China Sea
Ocean Data View

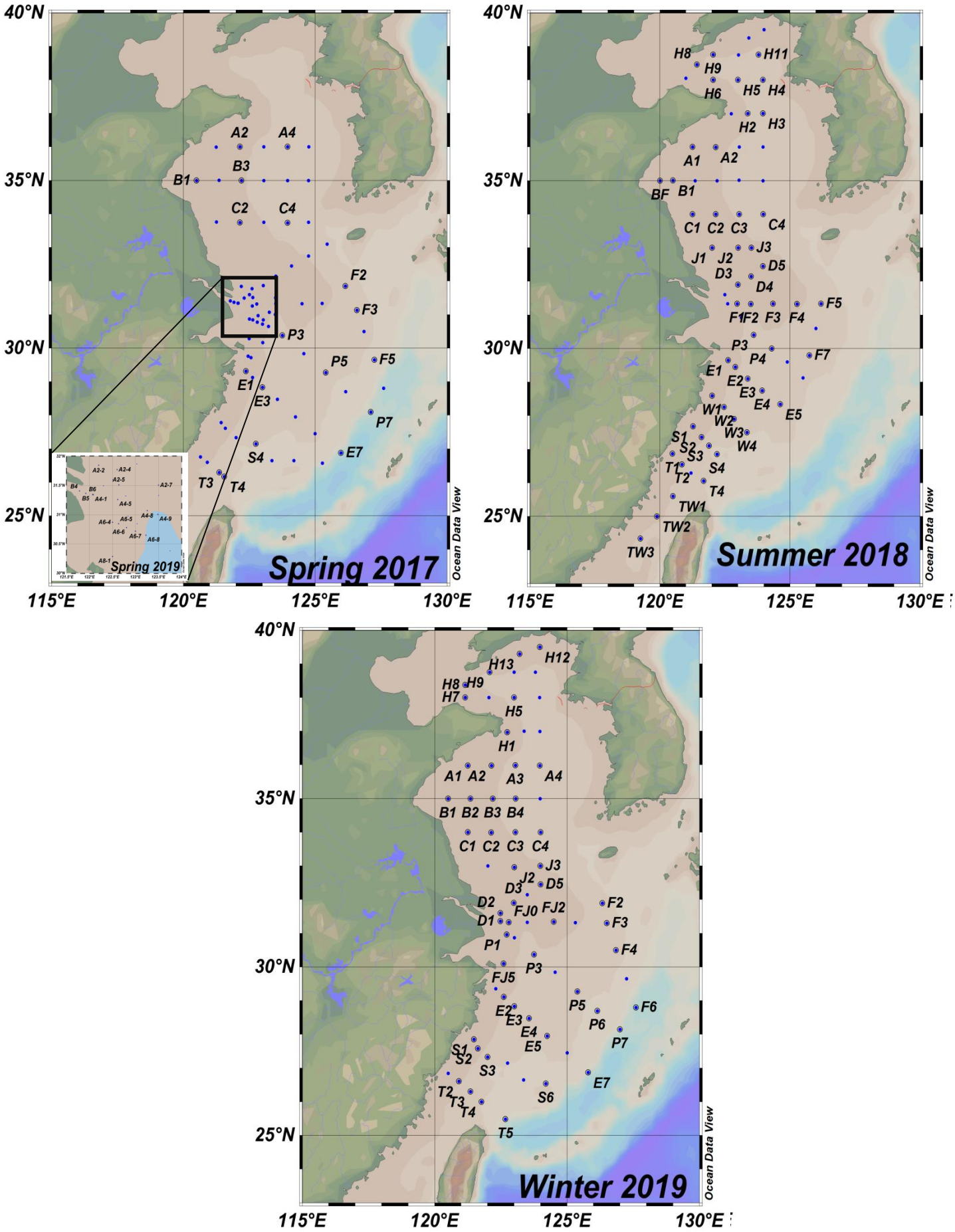

Fig. 1 Map of sampling stations.

2.2 Sampling

We collected 220 paired SML and SSW water samples. SSW samples were collected at 2–5 m depth using 24 × 10-L Niskin bottles mounted on a rosette equipped with a conductivity-temperature-depth (CTD) profiler. The SML samples were collected using the screen sampling technique (Chen et al., 2016; Garrett, 1965) and were taken directly from the ship's bow when conditions were calm. A screen sampler with a 1.6 mm mesh of stainless steel wire on a 40 cm × 40 cm stainless steel frame was used. The SML samples were collected in 500 mL brown sample bottles. The screen was held level and dipped into the sea surface, moved laterally in order to sample from an undisturbed film, and then withdrawn slowly from the surface. Repeated dipping (11 times, 600 ml) was conducted until the desired volume was collected (the depth of the SML sample is nearly 300 ~ 1000 um). The screen method is often applied during field studies because of its relatively short sampling time and large sample volume compared to other techniques (Momzikoff et al., 2004; Chen et al., 2016). Immediately after collection, samples were filtered using 0.7 μm glass fiber filters (GF/F, Whatmann) and the filtrates were transferred to 60 mL and 40 mL brown glass bottles (pre-cleaned and pre-combusted) for later CDOM and DOC analyses. All samples were frozen (-20 ℃) and protected from light, and upon arriving at the land laboratory, were analyzed as soon as possible. Sea surface temperature and salinity were obtained from a Seabird 911 CTD Rosette. Meteorological data (e.g., wind speed and air temperature) were recorded simultaneously by a ship-borne weather instrument (Li et al., 2019).

2.3 Photoexposure experiment

SSW and SML water samples were collected in July 2018 at stations A3, BF, and H10 as well as D2 and F6 located in the YS and the ECS, respectively. Samples (SSW: 2L; SML: 500 mL) were

134 immediately passed through 0.22 μm PES filters (Pall Corp. Port Washington, NY, USA) to remove
135 the majority of bacteria, placed in acid-washed and pre-combusted brown glass bottles and stored at
136 4 ℃. Similarly, filtered samples from each site were placed in five 80 mL optically transparent quartz
137 tubes (acid-washed and pre-combusted) and sealed without headspace or air bubbles to measure the
138 effect of light exposure. The quartz tubes were positioned on their sides under the irradiation source to
139 maximize the exposure of the sample; the water depth in each tube was 5 cm (i.e. the diameter of the
140 tube). Both sets (SML and SSW) were irradiated for 6, 12, 24, 50, and 88 h (25 ℃) in a GLZ-C
141 Quantum Sensor (Top Cloud-Agri Instrument, Zhejiang, China) solar simulator. All samples for DOC
142 concentration measurements were acidified to approximately pH 2.0 with high purity HCl and
143 analyzed within 7 d, and absorbance spectra and fluorescence excitation emission matrices (EEMs)
144 were run on non-acidified samples within 3 d of sampling (4 ℃ and dark).

145 *2.4 Analytical measurements*

146 *Determination of the CDOM absorption coefficient*

147 Absorption spectra were determined using a UV-visible spectrophotometer (UV-2550 bi-channel;
148 Shimadzu, Tokyo, Japan) equipped with two 10 cm path-length quartz cuvettes. Sample absorbance
149 was automatically corrected for the absorbance of Milli-Q water. Absorbance scans ranged from 200 to
150 800 nm, with a spectral resolution of 1 nm. The absorption coefficient of CDOM was calculated
151 according to equation (1):

152 $$a(\gamma) = 2.303A(\gamma)/l \quad (1)$$

153 where, A(λ) is the absorbance at wavelength λ; and r is the path length of the quartz cuvette in meters.

154 The spectral slope of the CDOM absorption curve (S) was calculated according to a non-linear
155 regression over the 275–295 nm and 350–400 nm wavelength range, according to:

156 $$a(\lambda) = a(\lambda_0)\exp[S(\lambda_0—\lambda)]+K \quad (2)$$

157 where, $\alpha(\lambda)$ is the absorption coefficient at wavelength λ; $\alpha(\lambda_0)$ is the absorption at the reference

wavelength λ_0 of 440 nm; S is the spectral slope; and K is a background parameter that accounts for baseline shifts or attenuation due to factors other than CDOM. S was measured in the wavelength ranges of 275–295 nm ($S_{275-295}$, nm^{-1}) and 350–400 nm ($S_{350-400}$, nm^{-1}). $S_{275-295}$ is used to characterize DOM, with high values generally indicative of low-molecular-weight DOM that are linked to photochemical modification (Helms et al., 2008; Ortega-Retuerta et al., 2009). The spectral slope ratio (S_R) was defined as the ratio of the two spectral slopes, $S_{275-295}$ to $S_{350-400}$. S_R is also a sensitive indicator of photochemically induced changes in the molecular weight within the CDOM pool, with increases in S_R suggesting stronger photochemical degradation (Helms et al., 2008; Ortega-Retuerta et al., 2009). We used the absorption coefficient at 254 nm (a(254)) to determine the concentration and distribution of CDOM in the SML from the eastern marginal seas of China. The specific UV absorbance ($SUVA_{254}$) can be used to measure aromaticity (Weishaar et al., 2003) and molecular weight (Chowdhury, 2013) of DOM, with higher values generally indicative of higher aromaticity. $SUVA_{254}$ is calculated as dividing the absorbance at 254 nm by DOC.

EEMs and determination of the CDOM fluorescence index

EEMs were obtained using a F-4500 fluorescence spectrophotometer with a 1 cm quartz cuvette (Shimadzu) (Hoge et al., 1993). The emission spectra were scanned every 5 nm from 250 nm to 550 nm, and at the excitation wavelengths between 200–400 nm at 5 nm intervals, with 5 nm slit widths for the excitation and emission modes. The FL Toolbox, which was developed by Wade Sheldon (University of Georgia) for MATLAB, was used to remove the Rayleigh and Raman scattering peaks using the Delaunay triangulation method (Zepp et al., 2004). The fluorescence intensities of the samples were corrected with Milli-Q water blank EEMs and then normalized to the water Raman integrated area maximum fluorescence intensities (Ex/Em = 350 nm/365–430 nm, 5 nm bandpass) (Coble et al., 1998; Singh et al., 2010). Raman units (RU) (Stedmon et al., 2007; Singh et al., 2010) were used as the units for the Raman peak areas of water when the excitation wavelength of 350 nm was used for correction. EEMs were modeled using PARAFAC in MATLAB 7.5 with the DOMFluor

toolbox (Stedmon and Bro, 2008).

$$X_{ijk} = \sum_{n=1}^{F} a_{in}\, b_{jn} c_{kn} + \varepsilon_{ijk} \quad (3)$$

where X_{ijk} is the fluorescence intensity of the *i*th sample at the *k*th excitation and *j*th emission wavelengths; a_{in} is directly proportional to the concentration (scores) of the nth fluorophore in the *i*th sample; b_{jh} and c_{kn} are the estimates of the emission and excitation spectra (loadings) of the nth fluorophore at wavelengths *j* and *k*, respectively; *F* is the number of components (fluorophores); and ε_{ijk} represents the unexplained variability of the model (Singh et al., 2010). Split-half analysis validation was used to determine the number of fluorescent components. The fluorescence intensity of each fluorescent component was evaluated (Fig. S2, Supporting Information, Table 1).

Determination of DOC, chlorophyll-a, heterotrophic bacterial abundance, dissolved oxygen, and other parameters

Concentrations of DOC were determined using the Shimadzu TOC-V_{CPH} total organic carbon analyzer with an injection volume of 80 μL. The accuracy of the test was ensured by measuring a deep seawater reference (Hansell Laboratory, University of Miami) every 10 samples. Two forms of reference water have been developed for DOC analysis. Deep-ocean water, collected at 2600 m in the Sargasso Sea and containing biologically refractory DOC, as well as low carbon water for testing instrument blanks are available to the U.S. and international communities of aquatic chemists (Hansell, 2013; measurement and analytical errors < 19%). The Chl-*a* concentration was determined by a fluorescence spectrophotometer (7200-000, Turner Designs, CA) after extraction in 90% acetone based on the procedure of Parsons et al. (1984). DO was determined by iodination using the Winkler titration method (Carpenter, 1964), the endpoint was determined using starch as a visual indicator. Salinity and temperature data were collected in situ by a conductivity-temperature-depth sensor. All phytoplankton samples were enumerated in triplicate according to Specification for Oceanographic Survey (State Bureau of Technical Supervision Bureau, 1992). Nutrient species concentrations were determined using an automatic analyzer (QuAAtro, Seal Analytical, Germany) (Grasshoff et al., 2007). All phytoplankton samples were enumerated in triplicate according to Specification for Oceanographic Survey (State Bureau of Technical Supervision Bureau, 1992). Heterotrophic bacterial abundance was measured by flow cytometry (Beckman Coulter FC500-MPL) as described by Marie et al. (1997).

Enrichment factors

The enrichment factor (EF) in the SML is defined as follows

$$EF = C_M / C_S \quad (4)$$

where C_M is the concentration of any substance in the SML; and C_S is its concentration in the SSW. If the EF of a substance is greater than 1.0, that substance is considered enriched, if it is less than 1.0, it is considered depleted (Chen et al., 2016).

2.5 Statistical analyses

The correlation coefficient (*R*) and probability (*P*) values were used to evaluate the goodness-of-fit. The correlation matrix, analysis of variance, and principal components analysis were conducted with SPSS version 18.0 (SPSS Inc., Chicago, IL, USA) to determine the possible relationships between the DOM parameters and environmental factors. A *P*-value $\leq$ 0.05 was considered significant. Regression analyses between the optical parameters of DOM and several biogeochemical parameters in the SSW and the SML samples were performed in the Table S1 and the Table S2, respectively.

3. Results and discussion

3.1 Distribution and chemical characterization of DOM in the SSW of the eastern marginal seas of China

The surface distributions of salinity, temperature, CDOM, DOC, Chl-*a*, and several optical parameters in the study area during spring, summer and winter are shown in Fig. S3 (SSW)-S4 (SML) (Supporting Information). There was a strong south-to-north temperature gradient, with warmer waters

in the ECS and cooler waters in the YS. Lower salinities were observed in the Changjiang Estuary and coastal waters. The lowest mean wind speed was observed in the summer of 2018 (Table 2). In spring and summer, the bacterial abundances were lower in the YS (spring mean concentration: 2.26 × 10^8 cells/L; summer mean concentration: 3.79 × 10^8 cells/L) than in the ECS (spring mean: 2.98 × 10^8 cells/L; summer mean: 7.64 × 10^8 cells/L), indicating that the warmer southern ECS had stronger biological activity in the SSW.

The a(254) value ranged from 1.08 to 19.28 m^{-1} in the SML and from 0.82 to 14.23 m^{-1} in the SSW during these three seasons. a(254) values in the Changjiang Estuary (spring: station D1 (4.13 m^{-1}); summer: station D2 (3.98 m^{-1}); winter: station D1 (3.14 m^{-1})) and the northern YS (spring: station A2 (4.26 m^{-1}); summer: station H11 (5.37 m^{-1}); winter: station H12 (5.95 m^{-1})) were generally higher than other stations. CDOM absorption values and DOC concentrations were decreased from the inshore to the offshore stations (Fig. S3 c)-d)). There were significantly negative linear correlations between salinity and a(254) in all cruises in the SSW ($p < 0.01$, Fig. 3), especially in the ECS, implying that freshwater run-off and seawater mixing played a more important role in determining CDOM distributions in the SSW. The strongest negative linear relationship observed between salinity and a(254) was observed in winter when the influence of terrestrial input in this study region was maximal. In addition, $SUVA_{254}$ ranged from 0.51 to 8.39 L mg C^{-1} m^{-1} in the SML. In comparison with the SML, the SSW exhibited lower variability in $SUVA_{254}$ values from 0.63 to 5.39 L mg C^{-1} m^{-1}, with higher values at the northern YS stations and Changjiang Estuary coastal stations (Fig. S3k)). According to the $SUVA_{254}$ trends observed by Massicotte et al. (2017), the DOM composition we observed in the SSW of the Changjiang Estuary ecosystem were more similar to the DOM measured in freshwater ecosystems than in the ocean. $SUVA_{254}$ underwent a sharp decrease from the Changjiang

Estuary ecosystem to the southeastern ECS, suggesting that aromatic and/or highly conjugated DOM moieties were degraded along the aquatic continuum from the Changjiang Estuary to the open ocean. Higher $S_{275–295}$ values were also observed in some off-shore stations (Fig. S4i)). These comparisons showed that the DOM pools of the Changjiang Estuary contained molecules that were more HMW-DOM and contained more aromatic compounds, CDOM in the SSW of the southeastern ECS, which was derived predominantly from an autochthonous origin (phytoplankton production and bacterial activity), clearly showed the presence of organic matter freshly released into sea (Yang et al., 2020). The detail of mixing behavior, biological and photolytic degradation of dissolved organic matter in the East China Sea and the Yellow Sea were discussed in our previous paper (Yang et al., 2020).

3.2 Fluorescence signature and factors controlling the composition of FDOM components in the SSW and the SML

FDOM properties can be used as the sensitive indicator of DOM processing and water mass. Four fluorescent components were identified by PARAFAC analysis with the DOM Fluor toolbox in MATLAB 7.5 (Stedmon and Bro, 2008), hereafter named C1, C2, C3, and C4 (Fig. S2). The humic-like C1 and C3 were categorized as two traditional types of humic-like fluorescent components (Coble 1996). Component 1 had primary fluorescence excitation and emission peaks at 345 nm and 455 nm, respectively, which was similar to terrestrial humic-like fluorophores in the visible region (peak C) (Osburn et al., 2012). Relative to C1, the fluorescence of C3 was blue-shifted and had fluorescence peaks at 385 nm emission and 315 nm excitation. The microbial humic-like component had a relatively shorter emission peak wavelength compared to the terrestrial humic-like PARAFAC

components previously identified in the open ocean (Catala et al., 2015). C2 exhibited Ex/Em maxima at 255 nm/310 (375) nm, which could be considered tyrosine-like fluorescence (Stedmon et al., 2003) and attributed to autochthonous and/or microbial FDOM. C4 had an excitation range of 280 nm with an emission peak at 335 nm, which corresponded to peak T of the amino-acid-like fluorescence of tryptophan, likely derived from in situ primary autochthonous substances and other fresh biological sources (Coble, 1996). The tryptophan-like C4 and the humic-like C1 and C3 in the SSW were all negatively correlated with salinity ($P < 0.01$, Table S1), but increased with the increasing DO level. These suggested that water mixing and microbial activity were important factors in determining geographical distributions of FDOM in the SSW (Breitburg, et al., 2018; Yamashita et al., 2017; Galgani and Engel, 2016). Moreover, the geographical distribution of humic-like C1 and protein-like components were more similar to that of the Chl-a concentration in the SML (Fig. 4 a, b, d). Such relationships suggested that the production of protein-like and humic-like FDOM with phytoplankton production and decay in the SML.

FDOM enrichment in the SML of all stations ranged between 0.5 and 11 (n = 225) and FDOM was more frequently enriched (C1: 89.6%; C2: 73.2%; C3: 91.8%; C4: 93.4% of all samples) than CDOM. The fluorescence intensity of the components in the SML samples decreased in the following order: tryptophan-like > tyrosine-like > terrestrial humic-like > marine humic-like; whereas those in the SSW samples decreased in the order: tyrosine-like > tryptophan-like > marine humic-like > terrestrial humic-like. The tryptophan-like component (C4) was mostly enriched in the SML samples with a median EF = 2.2 and a range from 0.2 and 8.0. The EF of C4 was clearly higher than other components in all seasons (Fig. 6b)), especially in summer, and the FDOM composition in the SML revealed a relatively higher proportion of autochthonous tryptophan-like FDOM than the SSW. It has

299 also been broadly recognized that tryptophan-like C4 in the particulate fraction is related to recent
300 primary production (Brym et al., 2014; Yamashita, 2014) and that phytoplankton excrete
301 tryptophan-like fluorophores (Romare-Castillo et al., 2010). Together, as already emphasized
302 previously, the variation observed for FDOM can be more related to that of Chl-a in the SML, these
303 observations suggested that the DOM enriched in the SML was made up of a relatively higher
304 proportion of marine autochthonous DOM than the SSW.
305
306 *3.3 DOM and biogenic molecules accumulation in the SML*
307 Up to 88% of our CDOM samples were enriched in the SML, with the median EF for a(254) of
308 1.3, ranging between 0.4 and 6.7. Concentrations of CDOM, FDOM, nutrients, bacterial abundance,
309 and Chl-*a* in the SML were correlated with their respective SSW concentrations (Fig. 5),
310 demonstrating that transport from the SSW to the SML is an important pathway. Furthermore, the
311 relatively higher CDOM absorption enrichment value in the SML were found at longer wavelengths
312 (Fig. 6a)) EF of a(355) > EF of a(254)). Marine DOM usually has higher absorption slope than
313 terrestrial DOM, and the higher slope (no matter it is $S_{320-412}$ or $S_{275-295}$), marine production of DOM
314 had the largest influence on the CDOM absorption properties in the longer wavelength range (Danhiez
315 et al., 2017) ($S_{320-412}$: DOM marine origin VS. $S_{275-295}$: terrestrial DOM).
316 Galgani and Engel (2016) also observed that amino acid-like fluorophores were highly enriched
317 in the SML, not only due to their amphiphilic properties, but also due to their local production in the
318 SML. Therefore, the marine local production might significantly affect the composition of DOM in the
319 SML. Additionally, the nutrients showed significantly higher EFs (NO_3^-: 3.41 ± 6.08, n = 41; NO_2^-:
320 3.57 ± 5.54, n = 52; PO_4^{3-}: 2.13 ± 2.74, n = 68; and SiO_3^{2-}: 6.53 ± 13.67, n = 13) than biological and
321 DOM parameters in the SML. The strong correlation between the SML and SSW concentrations of

322 NO_2^-, NO_3^-, and SiO_3^{2-} (Fig. 5) showed that the similar fundamental drivers are probably at work in
323 both compartments for these nutrients. For example, dissolved substances, particles, and
324 microorganisms were brought to the interface by simple diffusion, rising bubbles (Jarvis, 1967),
325 convection, and upwelling from sediments and subsurface water, and at the same time, the microlayer
326 is also a sink for fallout from the atmosphere (Duce et al., 1976). In addition, we also observed the
327 significant positive relationship between a(254) and Chl-*a* (R = 0.662, P < 0.01) in the SML during
328 spring, and the positive relationship between the EF of PO_4^{3-} and the EF of Chl-*a* (R = 0.319, P = 0.01,
329 Table 3). These observations indicated that spatial variation of CDOM concentrations were related to
330 Chl-a in the SML. The enrichment of inorganic nutrients would be an important factor influencing the
331 production and composition of phytoplankton-produced DOM (Carlson and Hansell, 2003) in the
332 SML. Therefore, phytoplankton growth, primary productivity rate, biological activity and marine
333 autochthonous DOM production would all be enhanced by the enriched nutrients in the SML.
334
335 a)

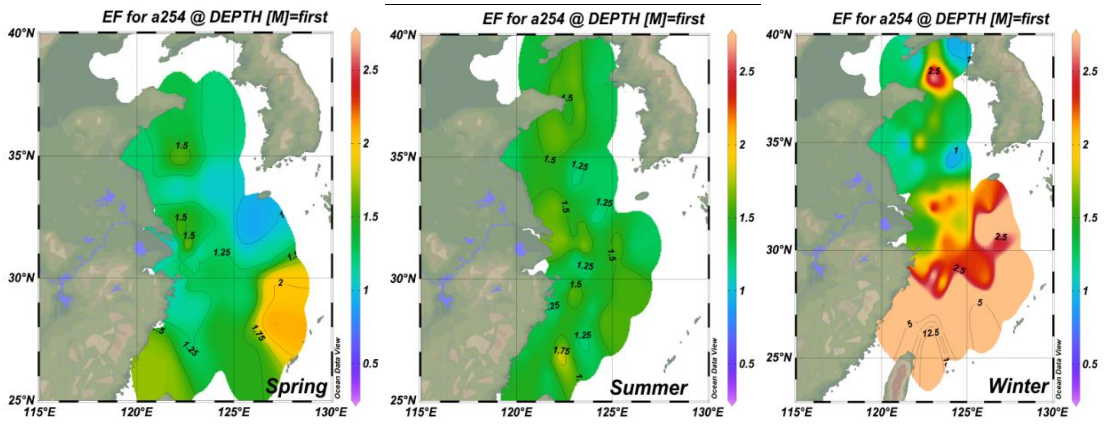

b)

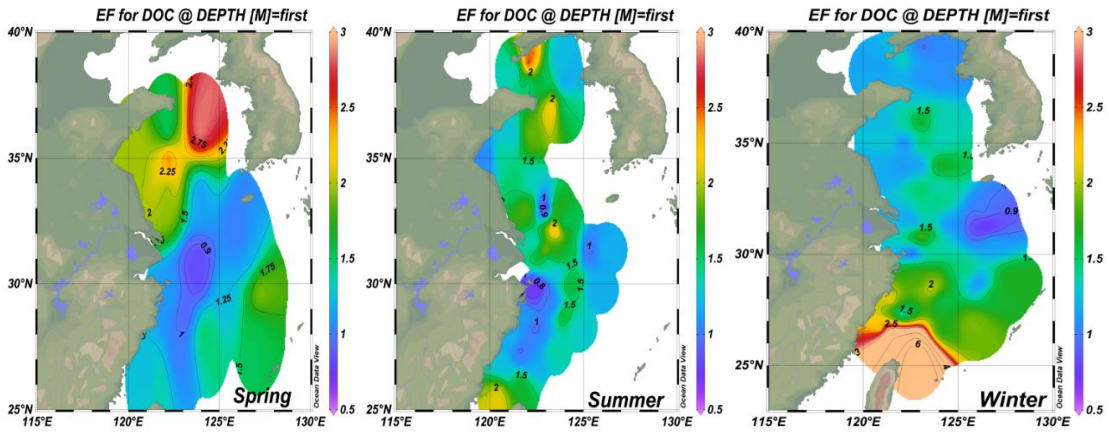

336

c)

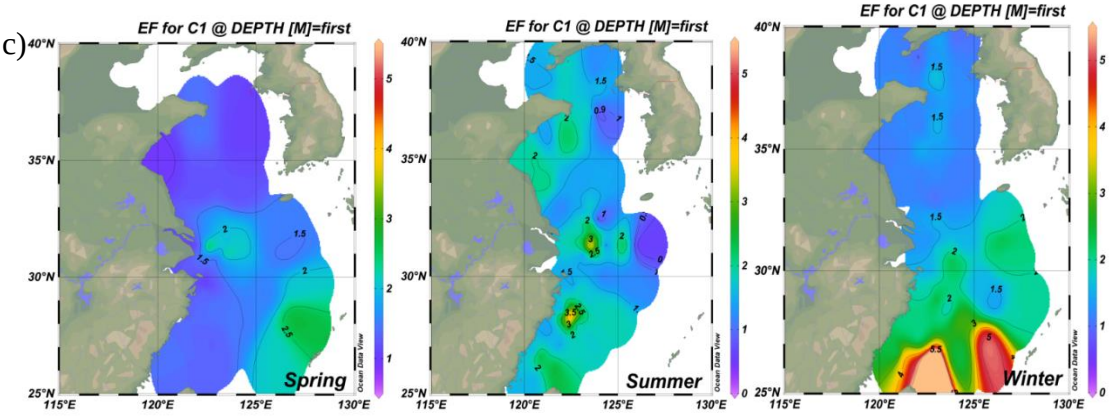

337

d)

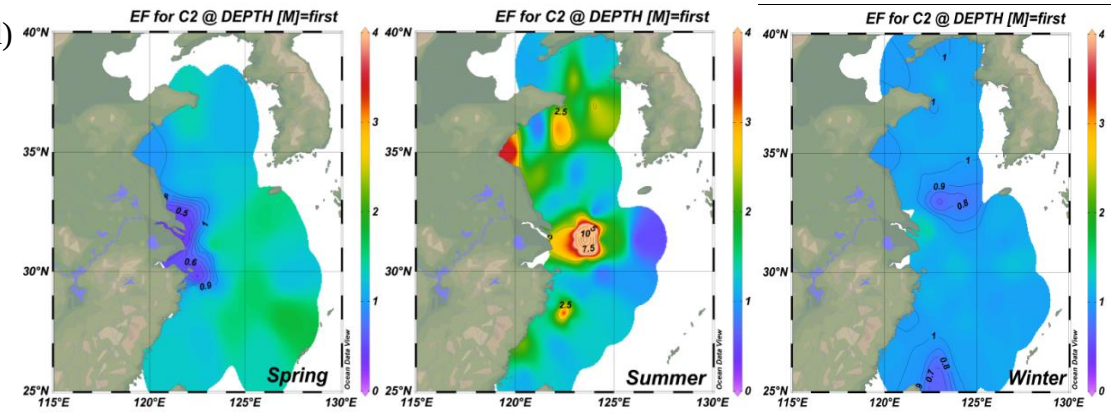

338

e)

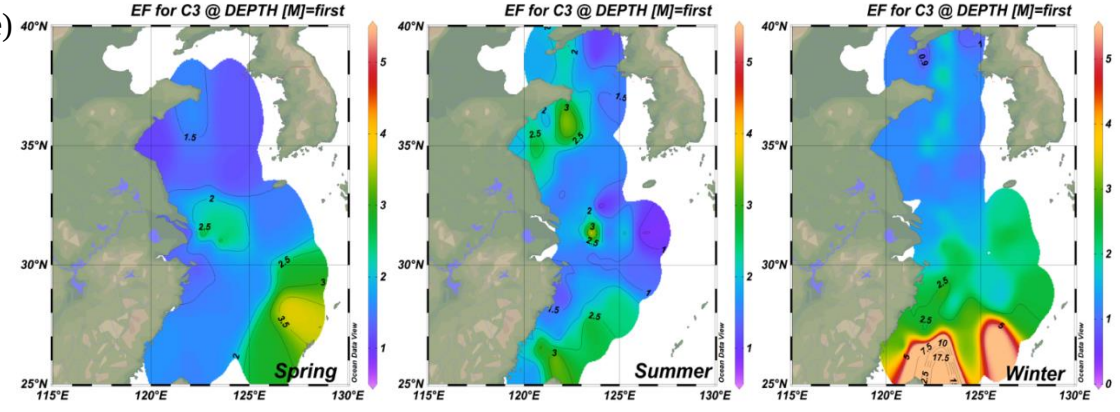

339

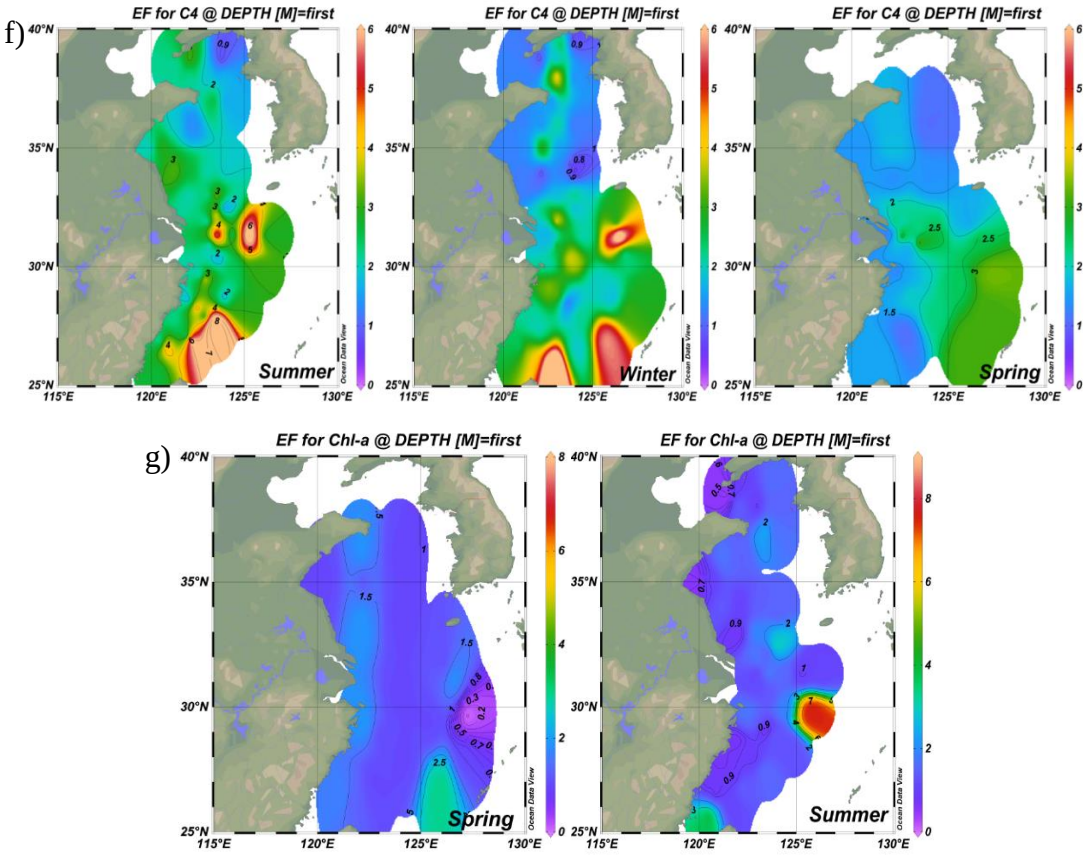

Fig. 2. Distributions of enrichment factors of CDOM, DOC, Chl-*a*, and four fluorescence components in the surface microlayer water during spring, summer, and winter. Increasing DOM yields were significant in coastal regions in all seasons, but the higher enrichment factors (EFs) were more pronounced in off-shore regions.

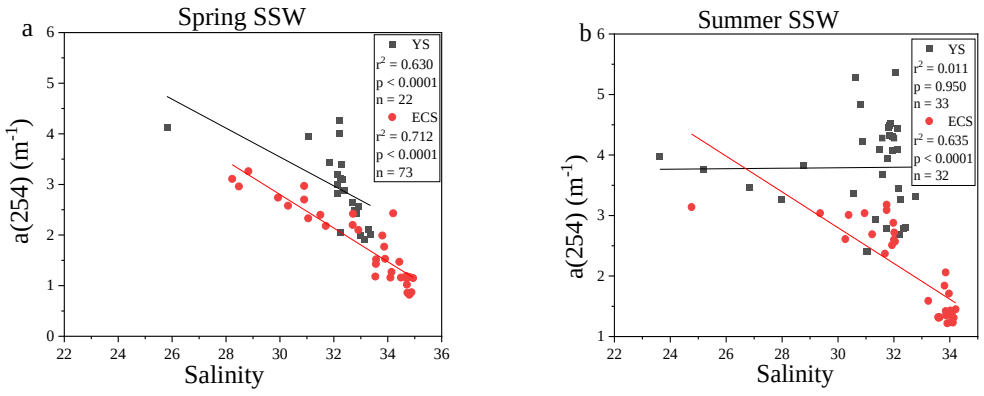

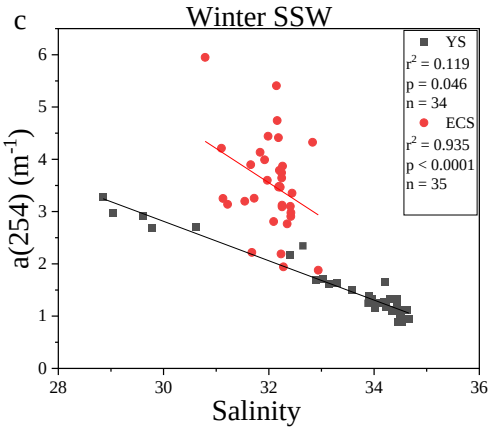

347

348 Fig. 3. Relationships between a(254) and salinity in the subsurface water (SSW) in the East China Sea
349 (ECS) and the Yellow Sea (YS) during spring, summer and winter.

350

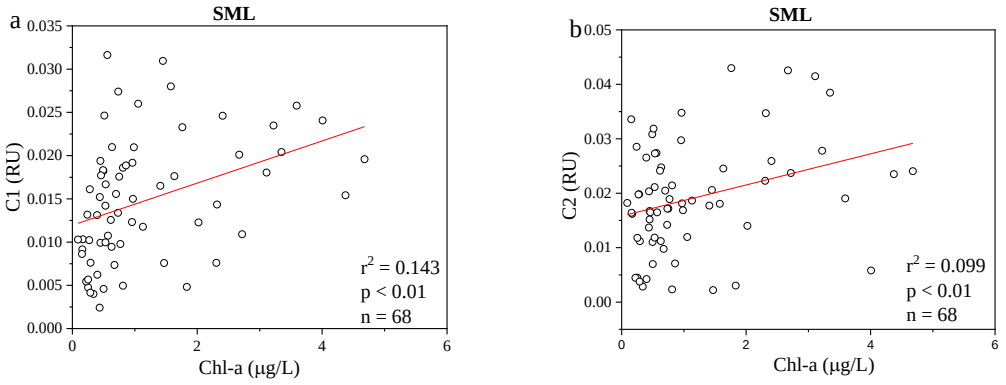

351

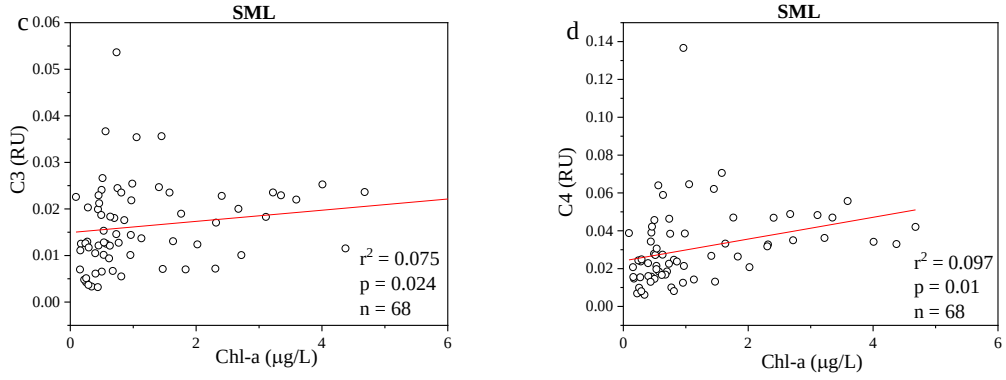

352

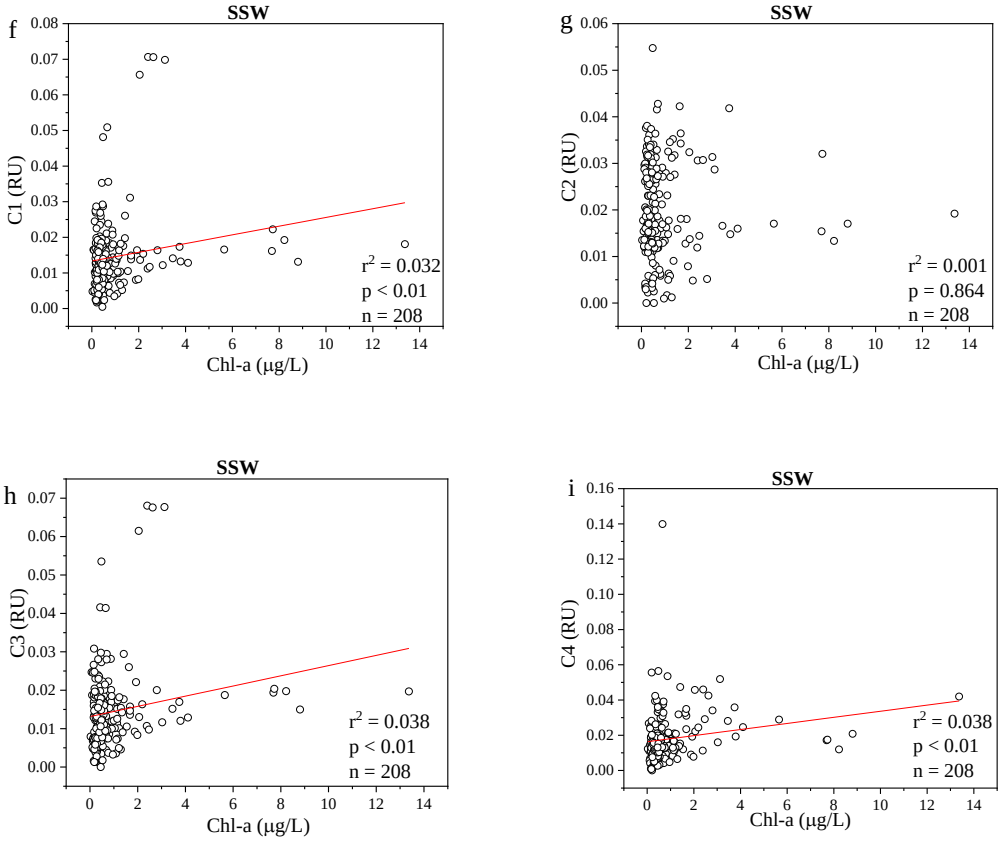

353

354

355 Fig. 4. Relationships between a(254), four fluorescence components and Chl-*a* in the sea-surface
356 microlayer (SML) (a-d) and in the SSW (f-i).

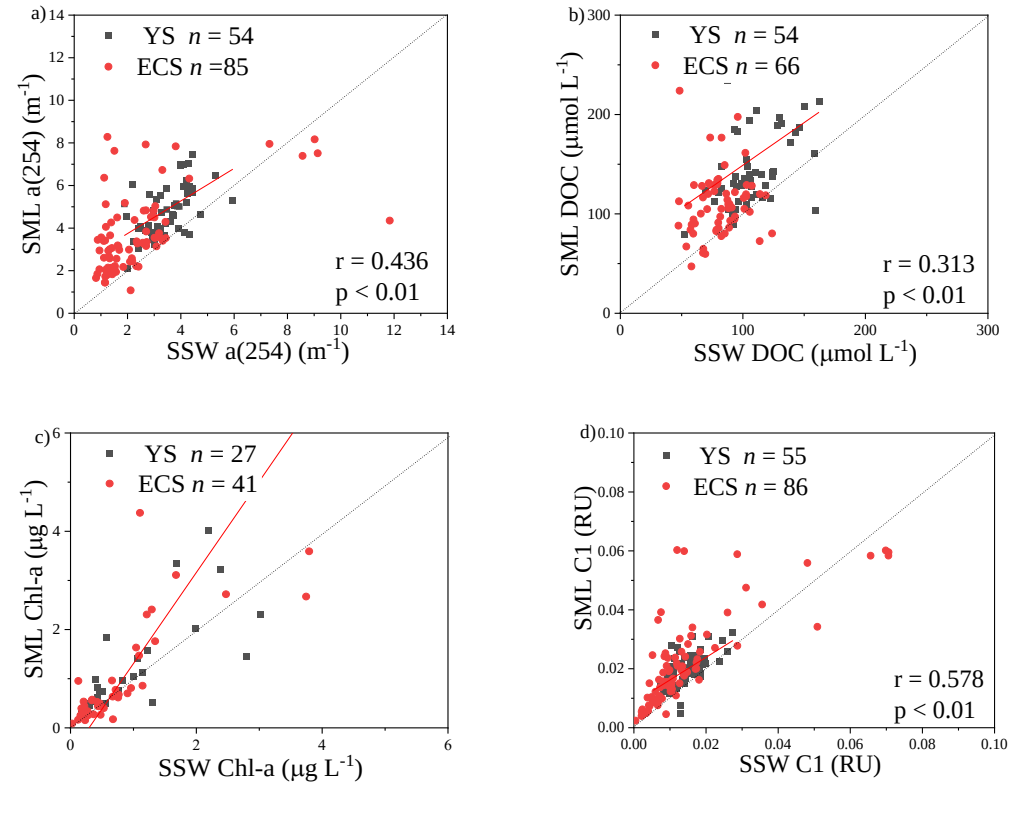

357

358

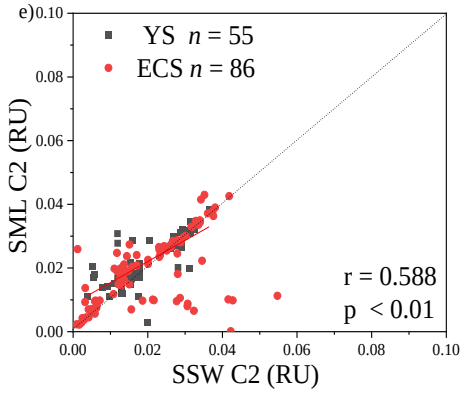

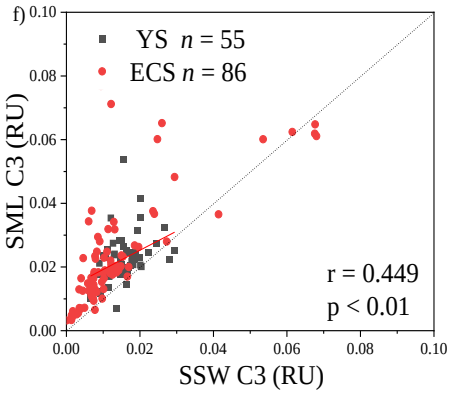

359

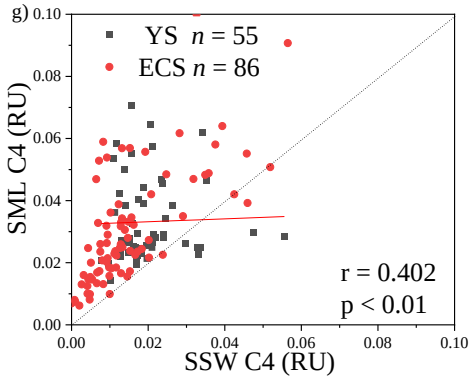

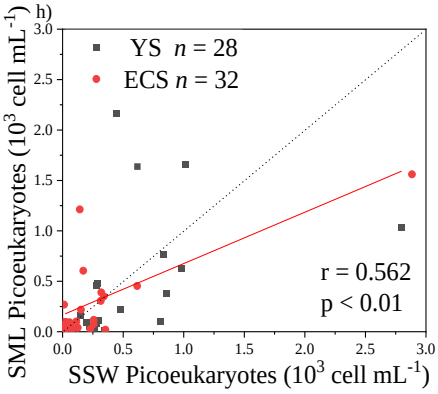

360

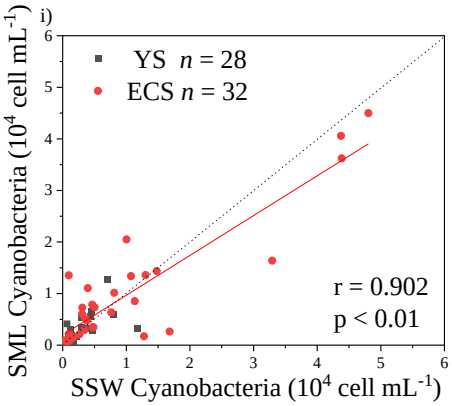

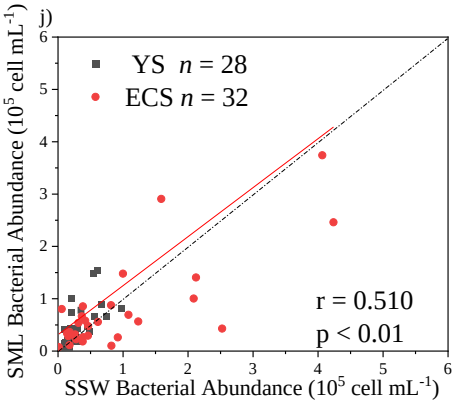

361

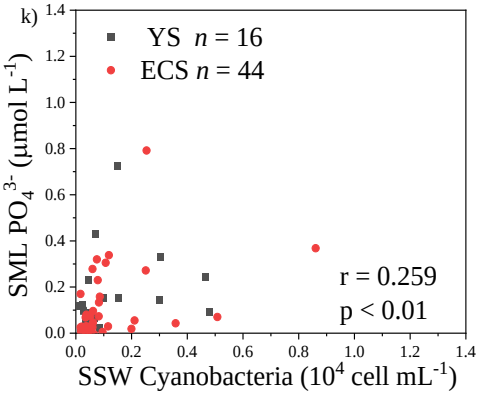

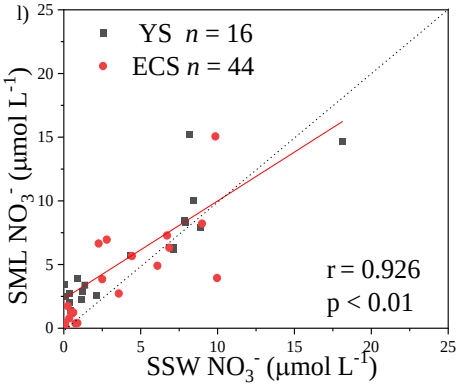

362

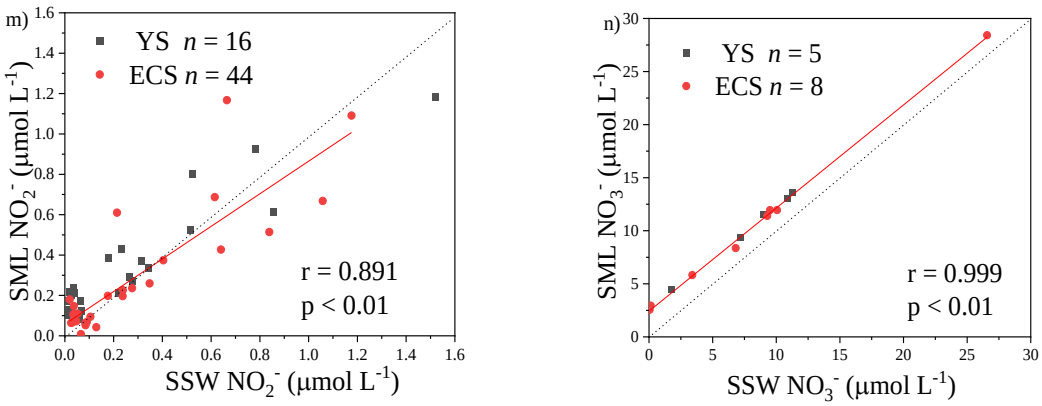

Fig. 5. Correlations between the microlayer CDOM, DOC, Chl-*a*, four fluorescence components concentrations, cyanobacteria, phytoplankton biomass, nutrients and bacterial abundance, and their subsurface water concentrations. The dashed lines correspond to the 1:1 lines, and the full lines are the regression models. (All DOM spectroscopic parameters sample were analyzed in spring, summer and winter; Chl-*a* was determined in spring, summer, and summer; cyanobacteria, phytoplankton biomass, nutrients and bacterial abundance were determined in spring and summer.).

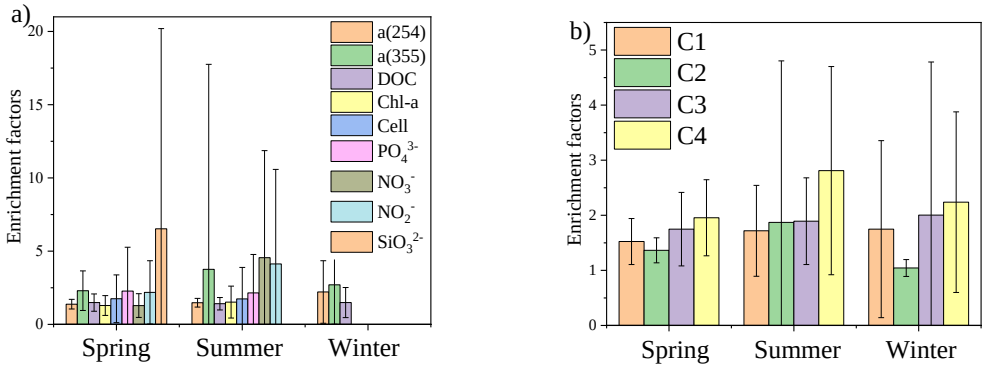

Fig. 6. Mean enrichment factor of a_{CDOM} (254 nm and 355 nm), DOC, Chl-*a*, nutrients (PO_4^{3-}; NO_3^-; NO_2^-, SiO_3^{2-}), and four fluorescence components during spring, summer, and winter.

3.4 Wind speed influencing the enrichment of DOM optical properties

The wind speeds during our observations ranged from 0.2 to 14.9 m s^{-1}. We divided them into three different wind regimes: low (0.0–2.0 m s^{-1}), moderate (2.0–10.0 m s^{-1}), and high (10.0–14.9 m s^{-1}). Although the EFs of DOC and Chl-*a* were negatively correlated with wind speed (DOC: $P = 0.002$; Chl-*a*: $P = 0.042$), the EFs of CDOM and FDOM were not. During the low wind regime, no significant relationships were apparent between wind speed and either EFs of CDOM or FDOM,

CDOM and FDOM were consistently enriched, with EFs ranging from 1.0 to 2.2, and a mean a(254) EF value of 1.3 (n = 20). However, the EFs during moderate winds had larger variability and ranged from 0.9 to 14.5, with a mean EF value of 1.6 (n = 143), and during high winds they ranged from 0.6 to 1.8, with a lower mean EF value of 1.1 (n = 18). In addition, depleted levels of CDOM (EF < 1) occurred at frequencies of 5.6%, 9.1%, and 20.0% during low, moderate, and high wind regimes, respectively. Therefore, although lower wind speeds and ascending bubbles might further promote the transportation of organic materials from the underlying waters, DOM enrichments were still observed at wind speeds up to > 10 m s^{-1}. Reinthaler et al. (2008) also reported that higher enrichment was found at higher wind speeds. During moderate to high wind regimes, breaking waves not only can disrupt the surface film and physically drive DOM back into the bulk water, but also facilitate the formation of the SML as rising bubble plumes transported DOM to the surface, resulting in wider ranges of EFs (Frew et al., 2004). Higher wind speed does enhance mixing (Reinthaler et al., 2008), which can arguably favour transport of nutrients and DOM from the SSW equally (Wurl et al., 2011). Although wind speed appear to play an important role in the enrichment of surface-active DOM, the chemical composition of the SML influence its stability. For example, enrichments of sulphate half-ester groups in the SML (Wurl and Holmes, 2008) could increase stability because these groups can influence the intrinsic viscosity of marine polymers (Nichols et al., 2005) and sulphur-containing algal carbohydrates are less soluble and hydrolysable (Kok et al., 2000). Sampling needs to be performed on the leeward side of the boat with the boat moving into the wind to aboid contamination. Although some disturbance of SML integrity was produced by the ship's movement and potential contamination at high wind speeds and tidal mixing. It has long been known that the SML reforms rapidly following physical disruption (Dragcevic and Pravdic, 1981). Rapid SML recovery occurs

because SML organics dispersed by breaking waves readily reabsorb to the surfaces of rising bubbles generated by the same breaking waves (Woolf, 2005). Enrichment processes and biochemical processes of organic substances in the marine environment are all likely to be the more important contributors of DOM to the SML in our study regions.

3.5 Photochemical degradation of DOM in the SSW and the SML

Photobleaching is one of the major mechanisms determining the geographical distributions of chromophoric and fluorescent DOM in the ocean (Helms et al., 2008; Brinkmann et al., 2003; Siegel et al., 2005). The average $SUVA_{254}$ values in SSW were generally higher than those in the SML in our study regions (SSW: 2.45 ± 0.91 L mg-C^{-1} m^{-1} vs. SML: 2.39 ± 1.34 L mg-C^{-1} m^{-1}), and the most obvious distinction happened in summer (Table 2). These indicated that although CDOM concentration in the SSW was lower than that in the SML, CDOM in the SSW has a higher degree of aromaticity compared to the SML. Thus we performed photochemical incubation experiments to confirm whether photochemical reactions influenced the differentiated aromaticity and photo-reactive features of DOM between the SML and the SSW.

After 88 h of exposure, the a(254) values were only 49.6%, 45.5%, 42.1%, 41.8% and 37.0% of the initial values at stations A3, BF, D2, F6, and H10 in the SSW, and 72.5%, 42.4%, 42.6%, 49.0% and 44.0% of the initial values at stations A3, BF, D2, F6, and H10 in the SML, respectively. Overall, a(254) and $SUVA_{254}$ decreased by 49.9 ± 12.8% and 43.0 ± 15.5%, respectively, in the SML, and by 56.8 ± 4.7% and 56.0 ± 10.2%, respectively in the SSW. Therefore, stimulated solar UV exposure caused a larger decrease in DOM absorbance in the SSW than the SML (Fig. 7). The relatively rapid decrease of $SUVA_{254}$ in the SSW indicated a more rapid conversion of DOM to less humic-type materials than in the SML. Although photodegradation causes CDOM absorption to decrease, DOC is

not sensitive to photodegradation in our photodegradation experiments (Fig. 7), implying that the light exposure preferentially removed the colored DOM rather than the non-colored DOM (Bittar et al., 2015). Approximately 65% of FDOM was lost during the irradiation experiment, except in the case of the tyrosine-like component 2 from the SML at the station H10, which increased slightly. Photoproduction of tyrosine-like components has been previously reported by Zhu et al. (2017), who suggested that the photochemical degradation of CDOM contributed to the release small amounts of tyrosine-like fluorophores. The tryptophan-like C4, humic-like C1 and C3 were more photodegradated in the SSW than in the SML (Fig. 7c), e), f)). For example, C1, C3 and C4 show a marked decrease in the SSW at the off-shore station F6. Because of the origin of CDOM at the station F6 remote from the direct terrestrial influence, the majority of CDOM at the station F6 was thought to be a by-product of net primary production. The present results showed that a large fraction of the total CDOM in the SSW at the off-shore station F6 is still potentially sensitive to photooxidation. As already referred previously, CDOM in the SSW showed higher $SUVA_{254}$ values, and higher percentages of humic-like DOM than in the SML. Therefore, the photochemically mediated shifts in DOM in the SSW were more pronounced than those in the SML in our incubation experiments, in terms of both absorption and fluorescence values.

This heterogeneity in the EFs and photochemical reactivities of FDOM components can be related to the chemical and structural nature, such as molecular weight, aromaticity or humification of FDOM enrichment processes. Hydrophilic, carboxylic acid-bearing DOM moieties are preferentially degraded by simulated sunlight (Brinkmann et al., 2003). The largest fractions of photolabile DOM are made up of aromatic carbon rings or high double bond equivalent molecules (Kujawinski et al., 2004; Gonsior et al., 2009). The humic-like C1 and C3, all of which exhibited significantly positive

relationships with $SUVA_{254}$ (< 0.001, Table 1) and shown higher aromaticity, were more prone to photochemical degradation (Fig. 7c), e), and f)). The tyrosine-like C2, as compared to other protein-like compounds, is generally considered more labile and susceptible to bacterial cycling and rapid consumption by microbiota (Medeiros et al., 2015). The SML experiences the most intense solar radiation, especially ultraviolet (UV) light (Obernosterer et al., 2005). Photochemical degradation may, therefore, be a sink for aromaticity fluorescent components in the SML, and be a source for the tyrosine-like C2. In addition, Blough (1997) discovered that photochemical production rates in the SML should lead to the more rapid oxidative turnover of materials at the interface and potentially to reactions and processes not observed in bulk waters. Therefore, differences in $SUVA_{254}$ values and photoreaction behavior between the SSW and the SML may also reflect that DOM in the SML was already photobleached, which resulted in the decrease of DOM aromaticity, CDOM in the SSW appeared to be more susceptible to photochemical degradation than CDOM in the SML. Together, photo-irradiation have the significant influence on the accumulation of protein-like DOM and depletion of aromatic organic compounds in the SML, and organic carbon might have undergone a more rapid cycling in the SML than the SSW.

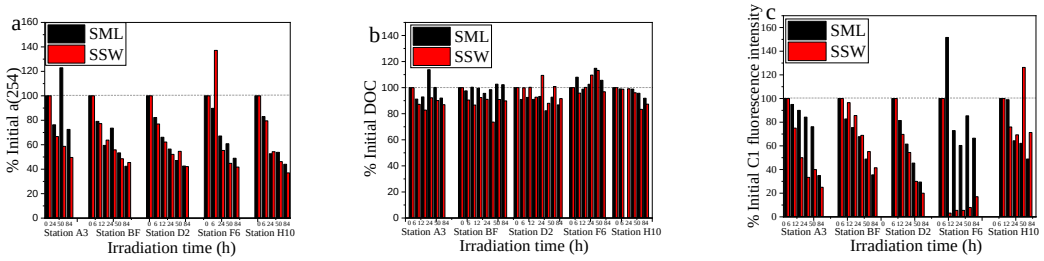

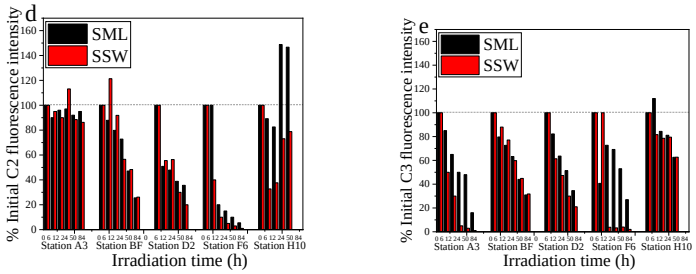

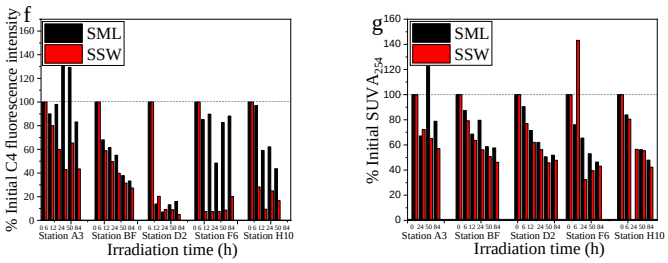

Fig. 7. Changes in ratios of a(254), DOC, $SUVA_{254}$ and four fluorescence components intensities to initial values for both SML and SSW sample.

3.6 Variations in the enrichment factors of CDOM, DOC, FDOM along the coastal regions to ocean

The concentrations of a(254) and DOC decreased from the coastal regions to the open ocean, and decreased from the northern part of the sampling area (the YS) to the southern part of the sampling area (the ECS) in both the SSW and the SML (Fig. S3 c)-d) and Fig. S4 a)-b)). However, CDOM and FDOM were more frequently enriched in the ECS (CDOM: 93% of all samples; FDOM: 72–94% of all samples) than that in the YS (CDOM: 86% of all samples; FDOM: 70–92% of all samples). The higher EF values for CDOM, FDOM, DOC, Chl-*a*, nutrients, and cell were generally observed in the ECS (Fig. 2). Lower EFs and EFs < 1, which indicate a depletion of CDOM in the SML, were usually observed at short distances from the coast (Fig. 2) with lower salinity. The salinity during our observations ranged from 23.6 to 35.1. Although CDOM and FDOM concentration negatively correlated with salinity, the EFs of CDOM and FDOM were weakly positive related with salinity (Fig. 8). The EFs of Chl-*a* and nutrient were also higher in the southeastern ECS (Fig. 2 and Fig. S5), where sufficient light and higher temperature combined to facilitate primary production and higher contributions of autochthonous materials to DOM. DOM in the SSW of the southern ECS was more dominated by marine autochthonous materials in our previous discussion (Yang et al., 2020). The Changjiang River discharges enormous amounts of N and P into the ECS (Liu et al., 2018), but

phosphorus is generally the major limiting element for phytoplankton growth in the ECS (Liu et al., 2016). Thus the difference in EFs of CDOM and Chl-a between YS and the ECS, and between the coast and off-shore regions is likely due to the significantly nutrients enrichment in the SML in the off-shore regions. In winter, we observed especially higher EF values for CDOM and FDOM in the southern ECS (Fig. 2a)-f)). With wind from the northwest (Weng et al., 2011), biologically essential trace elements and anthropogenic emissions are carried from the land and can enter the ocean via the SML by wet or dry deposition. The EFs of humic-like C1 and C3 were relatively high in winter (Fig. 6b)), probably due to the input from atmospheric deposition during winter, and the relatively low CDOM concentrations in bulk water. Atmospheric deposition of organic carbon and nutrients were found a peak in winter over the coastal ECS (Wang et al., 2019). We suggested that the EFs of CDOM and FDOM increased from the coastal regions to the open ocean, and increased from the YS to the ECS were likely due to the enrichment of enough nutrients in the SML in the open ocean promote phytoplankton biomass and DOM production.

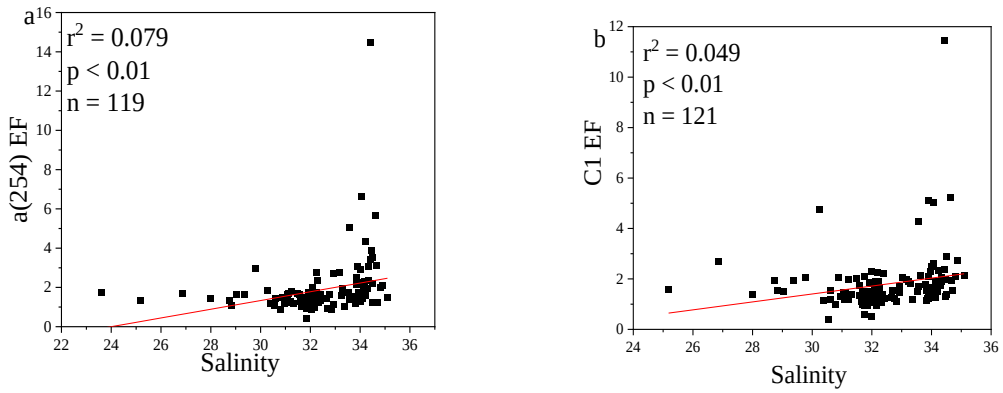

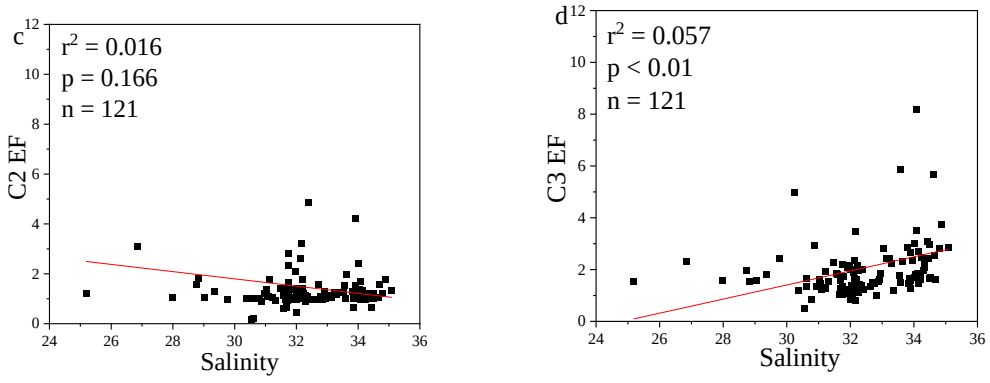

497

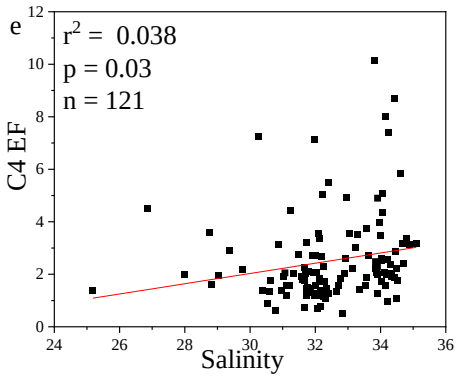

498

499 Fig. 8. Relationships between salinity and EFs of a(254), Chl-a, DOC, and four fluorescence
500 components.

The SML is an aggregate-enriched biofilm environment with distinct microbial communities, where the diversity of microorganisms can differ significantly from those of underlying waters (Liss and Duce, 2005; Cunliffe et al., 2013), the heterotrophic bacterial abundance in the SML was ~ 7.5 fold greater than those in the SSW in the ECS during our spring cruise (Sun et al., 2020). Here, EFs showed a greater presence of bacteria and marine protein-like DOM in the SML than that in the SSW, while the protein-like DOM was linked to microbial utilization and degraded faster than the humic-like substances (Yang et al., 2017; Jørgensen et al., 2011). Therefore, compared to coastal waters that have larger terrestrial DOM and nutrients inputs, CDOM shown higher EFs in off-shore regions where DOM in the SSW is mostly of marine autochthonous origin with higher temperatures and stronger biological activity. The significantly higher abundance of cells, phytoplankton, nutrients, and protein-like DOM in the SML supported microbial activities, and further contributing to the local release of marine extracellular DOM directly from microbes in the SML in the off-shore regions. When exposed to higher light intensities (summer), obviously enhance mineralization of DOM in the SML, and relatively less photochemical degradation in SSW could result in lower percentage of aromatic DOM in SML than the SSW. We concluded that SML CDOM dynamics can be expressed as a complex balance among enrichment process, primary production and photochemical destruction. Thus, higher EF of DOM in the SML in off-shore regions are likely supported by a favorable combination of: 1) deposition and accumulation of amphiphilic compounds, 2) importance of bubble for upward transport of DOM and enrichment in SML, and 3) new production of DOM within the SML as a consequence of higher nutrients enrichment and the primary production.

4. Conclusions

This study has provided the first data set that considers the distributions of CDOM, FDOM, DOC, Chl-*a*, nutrients, and bacterial abundances in the SML and SSW of the ECS and the YS during spring, summer, and winter. We have observed that the CDOM distribution related variability in primary production in the SML. Furthermore, we have demonstrated that localized and stronger photochemical oxidation may be responsible for the decrease in the aromaticity of the DOM in the SML, due to enhanced transformation or removal of terrestrial DOM, compared with the SSW. We also demonstrated that in off-shore seawaters away from terrigenous influence, the EFs of CDOM, DOC, FDOM and Chl-a in SML tend to be higher in off-shore regions than those in coastal regions, because of the relatively higher enrichment of nutrients which could enhance phytoplankton growth and promoted plant production and DOM production in the SML. Multiple observations of spatial distributions, seasonal variations, chemical compositions, and photochemical reactions of CDOM in the SML have supported the hypothesis that stronger enrichment and photochemical processes occur in the SML in ocean, resulting in relatively accelerated enrichment of more marine local production DOM in the SML than the SSW.

Acknowledgements

We thank the captain and crews of the R/V '*Dong Fang Hong 2*', the R/V '*Dong Fang Hong 3*', and the R/V '*Zhe Yu 2*' for their assistance and cooperation during the investigation. We gratefully acknowledge Ya-Hui Gao (Xiamen University), Yu Xin (Ocean University of China), and Xiao-Hua Zhang (Ocean University of China) for providing the Chl-*a*, nutrients, bacterial abundance and picoplankton data, respectively. This work was financially supported by the National Key Research and Development Program (Grant No. 2016YFA0601304), and the National Natural Science Foundation of China (Grant Nos. 41806093 and 491830534).

References

Aller, J.Y., Kuznetsova, M., Jahns, C.J., Kemp, P.F., 2005. The sea surface microlayer as a source of viral and bacterial enrichment in marine aerosols. J. Aerosol Sci. 36(5), 801–812. https://doi.org/10.1016/j.jaerosci.2004.10.012

Bittar, T.B., Vieira, A.A.H., Stubbins, A., Mopper, K., 2015. Competition between photochemical and biological degradation of dissolved organic matter from the cyanobacteria Microcystis aeruginosa. Limnol. Oceanogr. 2015, 60(4), 1172–1194. https://doi.org/10.1002/lno.10090

Breitburg, D., Levin, L.A., Oschlies, A., Grégoire, M., Chavez, F.P., Conley, D.J., Garçon, V., Gilbert, D., Gutiérrez, D., Isensee, K., Jacinto, G.S., Limburg, K.E., Montes, I., Naqvi, S.W.A., Pitcher, G.C., Rabalais, N.N., Roman, M.R., Rose, K.A., Seibel, B.A., Telszewski, M., Yasuhara, M., Zhang, J., Declining oxygen in the global ocean and coastal waters. Science 2018, 5, 359(6371), eaam7240. https://doi.org/10.1126/science.aam7240

Brinkmann, T., Sartorius, D., Frimmel, F.H., 2003. Photobleaching of humic rich dissolved organic matter. Aquat. Sci. 65(4), 415–424. https://doi.org/10.1007/s00027-003-0670-9

Brym, A., Paerl, H.W., Montgomery, M.T., Handsel, L.T., Ziervogel, K., Osburn, C.L., 2014. Optical and chemical characterization of base-extracted particulate organic matter in coastal marine environments. Mar. Chem. 162(6), 96–113. https://doi.org/10.1007/s00027-003-0670-9

Carlson, C.A., Hansell, D.A., 2003. The contribution of dissolved organic carbon and nitrogen to biogeochemistry of the Ross Sea. In: DiTullio, G., Dunbar, R. (Eds.), Biogeochemical Cycles in the Ross Sea. AGU Press, Washington DC, pp. 123–142.

Carpenter, J.H., 1964. The Chesapeake Bay Institute technique for the Winkler dissolved oxygen

method. Limnol. Oceanogr. 10(1964), 141–143. https://doi.org/10.4319/lo.1965.10.1.0141

Catala, T.S., Reche, I., Fuenteslema, A., Romeracastillo, C., Nietocid, M., Ortegaretuerta, E., Alvarezsalgado, X.A., 2015. Turnover time of fluorescent dissolved organic matter in the dark global ocean. Nat. Com. 6(1), 5986–5993. https://doi.org/10.1038/ncomms6986

Chen, Y., Yang, G., Xia, Q., Wu, G., 2016. Enrichment and characterization of dissolved organic matter in the surface microlayer and subsurface water of the South Yellow Sea. Mar. Chem. 182(Mar. 20), 1–13. https://doi.org/10.1016/j.marchem.2016.04.001

Chowdhury, S., 2013. Trihalomethanes in drinking water: Effect of natural organic matter distribution. Water SA 39(1), 1–7. https://doi.org/10.4314/wsa.v39i1.1

Coble, P.G., 1996. Characterization of marine and terrestrial DOM in seawater using excitation-emission matrix spectroscopy. Mar. Chem. 51(4), 325–346. https://doi.org/10.1016/0304-4203(95)00062-3

Coble, P.G., 2007. Marine optical biogeochemistry: the chemistry of ocean color. Chem. Rev. 107(2), 402–418. https://doi.org/10.1002/chin.200720265

Cunliffe, M., Engel, A., Frka, S., Gasparovic, B., Guitart, C., Murrell, J.C., Wurl, O., 2013. Sea surface microlayers: A unified physicochemical and biological perspective of the air–ocean interface. Prog. Oceanogr. 109(Feb.), 104–116. https://doi.org/10.1016/j.pocean.2012.08.004

Danhiez, F.P., Vantrepotte, V., Cauvin, A., Lebourg, E., Loisel, H., 2017. Optical properties of chromophoric dissolved organic matter during a phytoplankton bloom. Implication for DOC estimates from CDOM absorption. Limnol. Oceanogr. 62(4), 1409–1425. https://doi.org/10.1002/lno.10507

Dragcevic, D., Pravdic, V., 1981. Properties of the seawater-air interface. 2. Rates of surface film formation under steady state conditions. Limnol. Oceanogr. 26, 492–499.

https://doi.org/10.1016/0198-0254(81)91185-7

Duce, R.A., Hoffman, G.L., Ray, B.J., Fletcher, I.S., Wallace, G.T., Fasching, J.L., Piotrowicz, S.R., Walsh, P.R., Hoffman, E.J., Miller, J.M., Heffter, J.L., 1976. Trace metals in the marine atmosphere: Sources and fluxes, in: Marine Pollutant Transfer (H. L. Windom and R. A. Duce, eds.), pp. 77–119, Lexington Books, Lexington.

Engel, A., Galgani, L., 2016. The organic sea-surface microlayer in the upwelling region off the coast of Peru and potential implications for air–sea exchange processes. Biogeosciences 13(4), 989–1007. https://doi.org/10.5194/bg-13-989-2016

Frew, N.M., Bock, E.J., Schimpf, U., Hara, T., Hausecker, H., Edson, J.B., Jahne, B., 2004. Air-sea gas transfer: Its dependence on wind stress, small-scale roughness, and surface films. J. Geophys. Res.-Oceans 109(C8), S17. https://doi.org/10.1029/2003JC002131

Galgani, L., Engel, A., 2016. Changes in optical characteristics of surface microlayers hint to photochemically and microbially mediated DOM turnover in the upwelling region off the coast of Peru. Biogeosciences 13(8), 2453–2473. https://doi.org/10.5194/bg-13-2453-2016

Garrett, W.D., 1965. Collection of slick-forming materials from the sea surface. Limnol. Oceanogr. 10(1965), 602–605. https://doi.org/10.2307/2833459

Gonsior, M., Peake, B.M., Cooper, W.T., Podgorski, D., D'Andrilli, J., Cooper, W.J., 2009. Photochemically induced changes in dissolved organic matter identified by ultrahigh resolution fourier transform ion cyclotron resonance mass spectrometry. Environ. Sci. Technol. 43(3), 698–703. https://doi.org/10.1021/es8022804

Grasshoff, K., Kremling, K., Ehrhardt, M., 2007. Methods of Seawater Analysis, 3rd. Edition. pp. 407–420.

Guo, W., Yang, L., Zhai, W., Chen, W., Osburn, C.L., Huang, X., Li, Y., 2014. Runoff-mediated

seasonal oscillation in the dynamics of dissolved organic matter in different branches of a large bifurcated estuary-The Changjiang Estuary. J. Geophys. Res.-Biogeosciences 119, 776–793. https://doi.org/10.1002/2013JG002540

Hansell, D.A., 2013. Dissolved organic carbon reference material program. Eos Transactions American Geophysical Union, 86(35), 308. https://doi.org/10.1029/2005EO350003

Hardy, J.T., 1982. The sea surface microlayer: Biology, chemistry and anthropogenic enrichment. Prog. Oceanogr. 11(4), 307–328. https://doi.org/10.1016/0079-6611(82)90001-5

Hardy, J.T., Apts, C.W., 1989. Photosynthetic carbon reduction: high rates in the sea-surface microlayer. Mar. Biol. 101(3), 411–417. https://doi.org/10.1007/BF00428138

Helms, J.R., Stubbins, A., Ritchie, J.D., Minor, E.C., Kieber, D.J., Mopper, K., 2008. Absorption spectral slopes and slope ratios as indicators of molecular weight, source, and photobleaching of chromophoric dissolved organic matter. Limnol. Oceanogr. 53(3), 955–969. https://doi.org/10.4319/lo.2008.53.3.0955

Hoge, F.E., Vodacek, A., Blough, N.V., 1993. Inherent optical properties of the ocean: retrieval of the absorption coefficient of chromophoric dissolved organic matter from fluorescence measurements. Limnol. Oceanogr. 38(7), 1394–1402. https://doi.org/10.4319/lo.1993.38.7.1394

Jarvis, N.L., 1967. Adsorption of surf ace-active material at the sea-air interface, Limnol. Oceanogr. 12, 213–221. https://doi.org/10.4319/lo.1967.12.2.0213

Jørgensen, L., Stedmon, C.A., Kragh, T., Markager, S., Middelboe, M., Søndergaard, M., 2011. Global trends in the fluorescence characteristics and distribution of marine dissolved organic matter. Mar. Chem. 126(1–4), 139–148. https://doi.org/10.1016/j.marchem.2011.05.002

635 Kieber, D.J., Mcdaniel, J., Mopper, K., 1989. Photochemical source of biological substrates in sea
636 water: implications for carbon cycling. Nature 341(6243), 637–639.
637 https://doi.org/10.1038/341637a0
638 Kok, M., Schouten, S., Sinninghe Damsté J.S., 2000. Formation of insoluble, nonhydrolyzable,
639 sulfur-rich macromolecules via incorporation of inorganic sulfur species into algal carbohydrates.
640 Geochim. Cosmochim. Acta 64(15), 2689–2699. https://doi.org/10.1016/S0016-7037(00)00382-3
641 Li, Y., He, Z., Yang, G., Wang, H., Zhuang, G., 2019. Volatile halocarbons in the marine atmosphere
642 and surface seawater: Diurnal and spatial variations and influences of environmental factors.
643 Atmos. Environ. 214, 116820. https://doi.org/10.1016/j.atmosenv.2019.116820
644 Liss, P.S., Duce, R.A., 1997. The Sea Surface and Global Change, Cambridge University Press, 519.
645 Liss, P.S., Duce, R.A., 2005. The Sea Surface and Global Change. Cambridge University Press: UK.
646 Liu, S.M., Qi, X.H., Li, X.N., Ye, H.R., Wu, Y., Ren, J.L., Zhang, J., Xu, W.Y., 2016. Nutrient
647 dynamics from the Changjiang (Yangtze River) estuary to the East China Sea. J. Mar. Syst.
648 154(Feb.), 15–27. https://doi.org/10.1016/j.jmarsys.2015.05.010
649 Liu, X., Beusen, A.H.W., Van Beek, L.P.H., Mogollón, J.M., Ran, X., Bouwman, A.F., 2018. Exploring
650 spatiotemporal changes of the Yangtze River (Changjiang) nitrogen and phosphorus sources,
651 retention and export to the East China Sea and Yellow Sea. Water Res. 142(Oct. 1), 246–255.
652 https://doi.org/10.1016/j.watres.2018.06.006
653 Margolin, A.R., Gonnelli, M., Hansell, D.A., Santinelli, C., 2018. Black sea dissolved organic matter
654 dynamics: insights from optical analyses. Limnol. Oceanogr. 63(3), 1425–1443.
655 https://doi.org/10.1002/lno.10791

Marie, D., Partensky, F., Jacquet, S., Vaulot, D., 1997. Enumeration and cell cycle analysis of natural populations of marine picoplankton by flow cytometry using the nucleic acid stain SYBR Green I. Appl. Environ. Microbiol. 63(1), 186–193. https://doi.org/10.1109/50.337494

Massicotte, P., Asmala, E., Stedmon, C., Markager, S., 2017. Global distribution of dissolved organic matter along the aquatic continuum: Across rivers, lakes and oceans. Sci. Total Environ. 609(Dec. 31), 180–191. https://doi.org/10.1016/j.scitotenv.2017.07.076

Mcknight, D.M., Boyer, E.W., Westerhoff, P., Doran, P.T., Kulbe, T., Andersen, D.T., 2001. Spectrofluorometric characterization of dissolved organic matter for indication of precursor organic material and aromaticity. Limnol. Oceanogr. 46(1), 38–48. https://doi.org/10.4319/lo.2001.46.1.0038

Medeiros, P.M., Seidel, M., Ward, N.D., Carpenter, E.J., Gomes, H.R., Niggemann, J., Dittmar, T., 2015. Fate of the Amazon River dissolved organic matter in the tropical Atlantic Ocean. Global Biogeochem. Cycl. 29(5), 677–690. https://doi.org/10.1002/2015GB005115

Mopper, K., Kieber, D.J., 2002. Photochemistry and the cycling of carbon, sulfur, nitrogen and phosphorus. In: Hansell DA, Carlson CA (eds) Biogeochemistry of dissolved organic matter. Academic Press, San Diego, pp. 455–507.

Momzikoff, A., Brinis, A., Dallot, S., Gondry, G., Saliot, A., Lebaron, P., 2004. Field study ofthe chemical characterization of the upper ocean surface using various samplers. Limnol. Oceanogr. Methods 2(11), 374–384. https://doi.org/10.4319/lom.2004.2.374

Nichols, C.M., Lardière, S.G., Bowman, J.P., Nichols, P.D., Gibson, J.A.E., Guézennec, J., 2005. Chemical Characterization of Exopolysaccharides from Antarctic Marine Bacteria. Microb. Ecol. 49(4), 578–589. https://doi.org/10.1007/s00248-004-0093-8

678 Obernosterer, I., Catala, P., Reinthaler, T., Herndl, G.J., Lebaron, P., 2005. Enhanced heterotrophic
679 activity in the surface microlayer of the Mediterranean Sea. Aquat. Microb. Ecol. 39(3), 293–302.
680 https://doi.org/10.3354/ame039293
681 Ogawa, H., Amagai, Y., Koike, I., Kaiser, K., Benner, R., 2001. Production of refractory dissolved
682 organic matter by bacteria. Science 292(5518), 917–920.
683 https://doi.org/10.1126/science.1057627
684 Orellana, M.V., Matrai, P.A., Leck, C., Rauschenberg, C.D., Lee, A.M., Coz, E., 2011. Marine
685 microgels as a source of cloud condensation nuclei in the high Arctic. Proc. Natl. Acad. Sci.
686 108(33), 13612–13617. https://doi.org/10.1073/pnas.1102457108
687 Ortega-Retuerta, E., Passow, U., Duarte, C.M., Reche, I., 2009. Effects of ultraviolet B radiation on
688 (not so) transparent exopolymer particles. Biogeosciences 6(12), 3071–3080.
689 https://doi.org/10.5194/bg-6-3071-2009
690 Osburn, C.L., Handsel, L.T., Mikan, M.P., Paerl, H.W., Montgomery, M.T., 2012. Fluorescence
691 tracking of dissolved and particulate organic matter quality in a river-dominated estuary. Environ.
692 Sci. Technol. 46(16), 8628–8636. https://doi.org/10.1021/es3007723
693 Parsons, T.R., Matia, Y., Lalli, C.M., 1984. A Manual of Chemical and Biological Methods for
694 Seawater Analysis. Pergamon Press, Oxford.
695 Reinthaler, T., Sintes, E., Herndl., G.J., 2008. Dissolved organic matter and bacterial production and
696 respiration in the sea-surface microlayer of the open Atlantic and the western Mediterranean sea.
697 Limnol. Oceanogr. 53(1), 122–136. https://doi.org/10.4319/lo.2008.53.1.0122
698 Romera-castillo, C., Sarmento, H., Alvarezsalgado, X.A., Gasol, J.M., Marrase, C., 2010. Production
699 of chromophoric dissolved organic matter by marine phytoplankton. Limnol. Oceanogr. 55(1),
700 446–454. https://doi.org/10.4319/lo.2010.55.1.0446

Sabbaghzadeh, B., Upstill-Goddard, R.C., Beale, R., Pereira, R., Nightingale, P.D., 2017. The Atlantic Ocean surface microlayer from 50 °N to 50 °S is ubiquitously enriched in surfactants at wind speeds up to 13 m s^{-1}. Geophys. Res. Lett. 44(6), 2852–2858. https://doi.org/10.1002/2017GL072988

Siegel, D.A., 2005. Colored dissolved organic matter and its influence on the satellite‐based characterization of the ocean biosphere. Geophys. Res. Lett. 32(20), 469–496. https://doi.org/10.1029/2005GL024310

Singh, S., D'Sa, E., Swenson, E., 2010. Seasonal variability in CDOM absorption and fluorescence properties in the Barataria Basin, Louisiana, USA. J. Environ. Sci. 22(10), 1481–1490. https://doi.org/10.1016/S1001-0742(09)60279-5

State Bureau of Technical Supervision Bureau, 1992. Specifications for Oceanographic Survey-Survey of Biology in Sea Water. Standard Press of China, Beijing, pp. 17–20.

Stedmon, C.A., Bro, R., 2008. Characterizing dissolved organic matter fluorescence with parallel factor analysis: a tutorial. Limnol. Oceanogr.-methods 6(11), 572–579. https://doi.org/10.4319/lom.2008.6.572b

Stedmon, C.A., Markager, S., 2005. Resolving the variability in dissolved organic matter fluorescence in a temperate estuary and its catchment using PARAFAC analysis. Limnol. Oceanogr. 50(2), 686–697. https://doi.org/10.4319/lo.2005.50.2.0686

Stedmon, C.A., Markager, S., Bro, R., 2003. Tracing dissolved organic matter in aquatic environments using a new approach to fluorescence spectroscopy. Mar. Chem. 82(3–4), 239–254. https://doi.org/10.1016/s0304-4203(03)00072-0

Stedmon, C.A., Markager, S., Tranvik, L., Kronberg, L., Slätis, T., Martinsen, W., 2007. Photochemical production of ammonium and transformation of dissolved organic matter in the

Baltic Sea. Mar. Chem. 104(3–4), 227–240. https://doi.org/10.1016/j.marchem.2006.11.005

Su, Y., Hu, E., Feng, M., Zhang, Y., Chen, F., Liu, Z., 2017. Comparison of bacterial growth in response to photodegraded terrestrial chromophoric dissolved organic matter in two lakes. Sci. Total Environ. 579(Feb. 1), 1203–1214. https://doi.org/10.1016/j.scitotenv.2016.11.104

Sun, H., Zhang, Y.H., Tan, S., Zheng, Y.F., Zhou, S., Ma, Q.Y., Yang, G.P., Todd, J., Zhang, X.H., 2020. DMSP-Producing Bacteria Are More Abundant in the Surface Microlayer than Subsurface Seawater of the East China Sea. Microb. Ecol. 80(1), 350–365. https://doi.org/10.1007/s00248-020-01507-8

Wang, F., Feng, T., Guo, Z., Li, Y., Lin, T., Rose, N.L., 2019. Sources and dry deposition of carbonaceous aerosols over the coastal East China Sea: Implications for anthropogenic pollutant pathways and deposition. Environ. Pollut. 245(Feb.), 771–779. https://doi.org/10.1016/j.envpol.2018.11.059

Weishaar, J.L., Aiken, G.R., Bergamaschi, B.A., Fram, M.S., Fujii, R., Mopper, K., 2003. Evaluation of specific ultraviolet absorbance as an indicator of the chemical composition and reactivity of dissolved organic carbon. Environ. Sci. Technol. 37(20), 4702–4708. https://doi.org/10.1021/es030360x

Weng, H., Tian, R., Ji, Z., Yu, X., 2011. Potential relationships between atmospheric particulate matter transported by winter monsoons and red tides in the East China Sea. Sci. Bull. 56(3), 297–305. https://doi.org/10.1007/s11434-010-4209-x

Woolf, D.K., 2005. Bubbles and their role gas exchange, in The Sea Surface and Global Change, edited by P. S. Liss and R. A. Duce, pp. 173–205, Cambridge Univ. Press, U. K

Wotton, R.S., Preston, T.M., 2005. Surface Films: Areas of Water Bodies That Are Often Overlooked.

Bioscience 55(2), 137–145. https://doi.org/10.1641/0006-3568(2005)055[0137:SFAOWB]2.0.CO

Wurl, O., Wurl, E., Miller, L.A., Johnson, K., Vagle, S., 2011. Formation and global distribution of sea-surface microlayers. Biogeosciences 8(1), 121–135. https://doi.org/10.5194/bg-8-121-2011

Wurl, O., Holmes, M., 2008. The gelatinous nature of the sea-surface microlayer. Mar. Chem. 110(1–2), 89–97. https://doi.org/10.1016/j.marchem.2008.02.009

Yamashita, Y., Hashihama, F., Saito, H., Fukuda, H., Ogawa, H., 2017. Factors controlling the geographical distribution of fluorescent dissolved organic matter in the surface waters of the Pacific Ocean. Limnol. Oceanogr. 62(6), 2360–2374. https://doi.org/10.1002/lno.10570

Yamashita, Y., 2004. In situ production of chromophoric dissolved organic matter in coastal environments. Geophys. Res. Lett. 31(14), 189–207. https://doi.org/10.1029/2004GL019734

Yang, L., Zhang, J., Yang, G.P., 2020. Mixing behavior, biological and photolytic degradation of dissolved organic matter in the East China Sea and the Yellow Sea. Sci. Total Environ. 762(6), 143164. https://doi.org/10.1016/j.scitotenv.2020.143164

Yang, L., Zhuang, W., Chen, C.A., Wang, B., Kuo, F., 2017. Unveiling the transformation and bioavailability of dissolved organic matter in contrasting hydrothermal vents using fluorescence EEM-PARAFAC. Water Res. 111(Mar. 15), 195–203. https://doi.org/10.1016/j.watres.2017.01.001

Zepp, R.G., Sheldon, W.M., Moran, M.A., 2004. Dissolved organic fluorophores in southeastern US coastal waters: correction method for eliminating Rayleigh and Raman scattering peaks in excitation–emission matrices. Mar. Chem. 89(1), 15–36. https://doi.org/10.1016/j.marchem.2004.02.006

Zhu, W.Z., Yang, G., Zhang, H., 2017. Photochemical behavior of dissolved and colloidal organic

768 matter in estuarine and oceanic waters. Sci. Total Environ. s607–608(Dec. 31), 214–224.
769 https://doi.org/10.1016/j.scitotenv.2017.06.163

Table 1 Spectral characteristics of the four fluorescent components identified by the PARAFAC modal in this study, compared with those preciously identified.

Component	Ex_{max} (nm)	Em_{max} (nm)	Coble (1996)	Comparison with other studies using PARAFAC	Description and probable source
C1	345	455	peak C 320-360/420-480	Osburn et al. (2012)	Terrestrial-like humic substances
C2	255	310 (375)	peak A 230-260/380-460	Stedmon et al. (2003)	Tyrosine-like or marine humic-like substances
C3	315	385	peak M 290-310/370-420	Stedmon and Markager (2005)	Marine humic-like substances (biological degradation)
C4	280	335	peak T 270-280/340-350	Coble (1996)	Tryptophan-like; Non-Humic-like; Biological production in the water column

Table 2 Average temperature, salinity, wind speed, CDOM a(254), DOC, Chlorophyll-*a* (Chl-*a)*, dissolved oxygen (DO), $S_{275\text{-}295}$, S_R, and $SUVA_{254}$ of the SSW and SML in the YS and ECS during spring, summer, and winter.

		Spring		Summer		Winter	
	Water layer	mean	SD	mean	SD	mean	SD
Temperature (℃)	SSW	14.0	4.91	24.0	3.66	14.0	5.23
Salinity	SSW	32.5	1.92	31.7	2.17	32.7	1.41
Wind Speed ($m\ s^{-1}$)	SSW	5.98	2.86	5.47	2.51	6.09	2.52
DO ($mg\ L^{-1}$)	SSW	6.44	0.85	7.57	1.07	8.32	0.99
Chl-*a* ($\mu g\ L^{-1}$)	SSW	1.26	2.38	1.13	1.48	0.42	0.25
	SML	1.63	3.66	1.28	1.13	no data	
DOC ($\mu mol\ L^{-1}$)	SSW	91.3	25.7	109.4	33.55	88.4	22.51
	SML	132.9	77.4	145.7	49.8	131.3	91.1
a(254) (m^{-1})	SSW	3.20	2.49	3.10	1.34	2.52	1.26
	SML	3.70	1.98	4.05	1.66	4.74	2.50
$S_{275\text{-}295}$ (nm^{-1})	SSW	0.0201	0.0049	0.0188	0.0035	0.0207	0.0068
	SML	0.0222	0.0073	0.0178	0.0021	0.021	0.0055
S_R	SSW	1.723	1.026	1.731	1.557	1.521	0.52
	SML	1.095	0.218	1.361	0.296	1.416	0.214
$SUVA_{254}$ ($L\ mg\text{-}C^{-1}\ m^{-1}$)	SSW	2.067	0.664	2.244	0.671	3.008	0.949
	SML	1.911	0.768	1.951	0.359	2.992	1.034

Table 3 Correlation coefficients between EF of DOM optical properties, Chl-*a*, DOC, PO_4^{3-}, NO_3^-, NO_2^-, SiO_3^{2-}, Cyanobacteria, Picophytoplankton, Bacterial abundance.

	EF of a(254)	EF of DOC	EF of Chl-*a*	Ef of C1	EF of C2	EF of C3	EF of C4	EF of PO_4^{3-}	EF of NO_3^-	EF of NO_2^-	EF of SiO_3^{2-}	EF of Cyanobacteria	EF of picophytoplankton
EF of DOC	0.185												
EF of Chl-*a*	0.092	0.021											
Ef of C1	**.336****	0.047	-0.119										
EF of C2	0.163	0.073	-0.017	**.635****									
EF of C3	**.413****	0.179	-0.096	**.907****	**.557****								
EF of C4	**.319****	0.021	0.011	**.574****	**.368****	**.628****							
EF of PO_4^{3-}	0.129	0.267	**.319***	0.131	-0.037	0.139	0.087						
EF of NO_3^-	-0.065	-0.054	0.235	-0.037	-0.044	-0.027	-0.053	0.26					
EF of NO_2^-	0.15	0.208	**.307***	0.142	-0.017	0.192	0.035	**.571****	0.271				
EF of SiO_3^{2-}	**.634***	0.004	0.074	0.122	-0.101	0.305	0.151	0.205	-0.118	-0.141			
EF of Cyanobacteria	0.091	-0.017	0.028	-0.027	-0.105	-0.047	-0.052	0.218	0.027	**.755****	-0.286		
EF of Picophytoplankton	**.347****	0.0281	0.252	-0.067	-0.082	-0.077	0.025	0.218	-0.08	0.113	-0.327	0.081	
EF of Bacterial abundance	-0.036	-0.069	-0.063	-0.061	0.004	0.014	-0.093	-0.12	-0.026	-0.073	-0.099	**.730****	-0.064

** Correlation is significant at the 0.01 level (two-tailed)

* Correlation is significant at the 0.05 level (two-tailed)